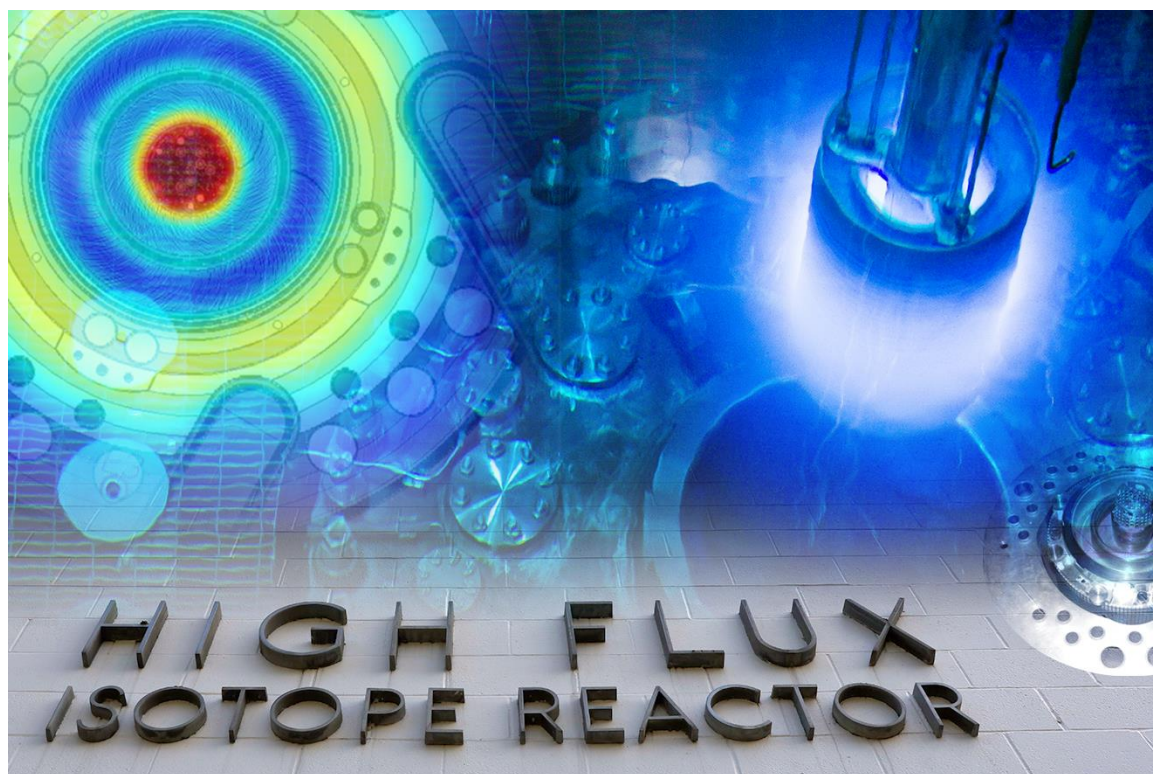# Volume 6: Experiment Facility Spectrum Tailoring

HFIR Futures – Enhanced Capabilities Series

David Chandler
Anne Campbell
Yanwen Zhang
Charles Daily
Jianwei Hu
Zain Karriem
Jeff Powers

April 2023

OAK RIDGE
National Laboratory

EXPERIMENT FACILITY SPECTRUM TAILORING

VOLUME 6 OF THE HFIR FUTURES – ENHANCED CAPABILITIES SERIES

David Chandler
Anne Campbell
Yanwen Zhang
Charles Daily
Jianwei Hu
Zain Karriem
Jeff Powers

April 2023

CONTENTS

LIST OF FIGURES

LIST OF TABLES

ABBREVIATIONS

ALD	associate laboratory director
ASME	American Society of Mechanical Engineers
BESAC	Basic Energy Sciences Advisory Committee
C/C	carbon/carbon
CE	control element
CL	centerline
CMC	ceramic matrix composite
CSA	concentrated solid-solution alloys
DOE	US Department of Energy
D-T	deuterium–tritium
EF	engineering slant tube facility
EG	experiment guide
EOC	end of cycle
FM	ferritic-martensitic
FTT	flux trap target
HEA	high-entropy alloy
HEU	highly enriched uranium
HFIR	High Flux Isotope Reactor
[HFIR]-CRITICAL	Critical Reactor Improvements Towards Increased and Continued Advanced Lifetime
[HFIR]-SCIENCE	Scientific Excellence through Neutron Capabilities Enhancement
[HFIR]-SENSe	Sustaining and Enhancing Neutron Science
HFTM	High Flux Test Module
HTR	high-temperature reactor
IBA	ion beam analysis
IBML	Ion Beam Materials Laboratory
IFE	inner fuel element
IFMIF	International Fusion Materials Irradiation Facility
ISVXF	inner small VXF
LDRD	Laboratory Directed Research and Development
LEU	low-enriched uranium
LVXF	large VXF
MCNP	Monte Carlo N-Particle
NRA	nuclear reaction analysis
OD	outer diameter
OFE	outer fuel element
OLVXF	outer large VXF
ORIC	Oak Ridge Isochronous Cyclotron
ORNL	Oak Ridge National Laboratory
OSVXF	outer small VXF
PB	permanent beryllium (reflector)
PKA	primary knock-on atom
PWR	pressurized water reactor
R&D	research and development
RB	removable beryllium (reflector)
RBS	Rutherford backscattering spectrometry
SAR	safety analysis report
SC	Office of Science

SiC	silicon carbide
SPB	semi-permanent beryllium (reflector)
ToF-ERDA	time-of-flight elastic recoil detection
TRL	technology readiness level
TSR	technical safety requirement
UT	University of Tennessee
VXF	vertical experiment facility

ABSTRACT

In-core irradiation experiment research, such as materials and fuels irradiation research and radioisotope production, is one of the primary missions of Oak Ridge National Laboratory's (ORNL) versatile High Flux Isotope Reactor (HFIR). In support of the HFIR-Sustaining and Enhancing Neutron Science (SENSe) Initiative, a technically diverse group of ORNL irradiation research subject matter experts formed the Spectrum Tailoring Working Group, with the goal of developing a compendium of experiment facility concepts to enhance irradiation experiment conditions via neutron spectrum tailoring capabilities. The purpose of this report is to document the concepts developed in FY22 and the associated scientific justifications, identify potential facility sponsors, and estimate costs and schedules for each concept. This report documents the efforts performed in FY22, which may continue in FY23 or later pending the direction of the HFIR-SENSe Initiative and the interested sponsors.

1. INTRODUCTION

Major efforts are being pursued to ensure the High Flux Isotope Reactor (HFIR) operates safely, reliably, and at an exceptionally high-performance level well into the future to support domestic and international neutron science-based research and radioisotope production. In response to a recent US Department of Energy (DOE) Basic Energy Sciences Advisory Committee (BESAC) review, the HFIR-Sustaining and Enhancing Neutron Science (SENSe) Initiative was established to provide a preconceptual assessment of hardware, systems, and infrastructure required to sustain and enhance HFIR capabilities. This report focuses on in-core irradiation enhancements, with special emphasis on neutron spectrum tailoring capability enhancements in support of the HFIR-SENSe Initiative. This report documents the efforts performed in FY22 which may continue into FY23.

1.1   THE HFIR FUTURES – ENHANCED CAPABILITIES SERIES

The DOE Office of Science (SC) chartered a BESAC review to assess the scientific justification for a domestic high-performance reactor–based research facility, including specific recommendations for HFIR (BESAC 2020). The review determined that HFIR will have a critical role in the future of US neutron science research and recommended the immediate pursual of scientific enabling enhancements, including reactor pressure vessel replacement, conversion to low-enriched uranium (LEU) fuel, enhanced capabilities for in-core irradiations and neutron scattering research, modifications to the fuel assembly, and restoration of the flux intensity of the original 100 MW highly enriched uranium (HEU) operations.

In response to the BESAC report recommendations, an Oak Ridge National Laboratory (ORNL) -funded initiative was established to provide a preconceptual assessment of the hardware, systems, and infrastructure required to sustain and enhance HFIR capabilities. The HFIR-SENSe Initiative consists of three Laboratory Directed Research and Development (LDRD) projects assessing (1) Critical Reactor Improvements Towards Increased and Continued Advanced Lifetime (HFIR-CRITICAL), (2) non-neutron-scattering scientific capability enhancements, referred to as *HFIR-SCIENCE* for Scientific Excellence through Neutron Capabilities Enhancement, and (3) neutron scattering scientific capability enhancements. The report by Bryan and Chandler (2023) provides for more information regarding HFIR, the BESAC report recommendations, the HFIR-SENSe Initiative, and the goals of the three LDRDs.

The HFIR-SCIENCE LDRD includes analysis of the long-term future of nonscattering scientific capabilities at HFIR. This blue-sky engagement with subject matter experts across ORNL has yielded incremental improvement ideas and new, transformational capabilities in the form of 35 enhancement concepts presented by these leading experts. The 35 concepts were grouped into 13 separate working groups, with the goal of each group being to develop the concepts, build a scientific justification, identify potential facility sponsors, and estimate costs and schedules for each concept. The HFIR Futures – Enhanced Capabilities Series includes 13 comprehensive volumes documenting an overview of the series (V1) and the capability enhancements presented by the working groups (V2–V13). Table 1 provides a summary of the multi-volume series of working group reports.

Table 1. Summary of the HFIR Futures – Enhanced Capabilities Series

Volume	Report number	Volume title
1	ORNL/TM-2022/2691/V1	Volume 1: Introduction to the HFIR Futures — Enhanced Capabilities Series
2	ORNL/TM-2022/2691/V2	Volume 2: Hot Cells Connected to the Reactor Pool
3	ORNL/TM-2022/2691/V3	Volume 3: Online Insertion and Removal Facilities
4	ORNL/TM-2022/2691/V4	Volume 4: Detection Systems and Ultra-Cold Neutrons
5	ORNL/TM-2022/2691/V5	Volume 5: Flexible Flux Trap Configurations
6	ORNL/TM-2022/2691/V6	Volume 6: Experiment Facility Spectrum Tailoring
7	ORNL/TM-2022/2691/V7	Volume 7: Cryogenic Facility
8	ORNL/TM-2022/2691/V8	Volume 8: Epithermal and Fast Neutron Radiography Facility
9	ORNL/TM-2022/2691/V9	Volume 9: Critical Facility with Add-On Ion Beam
10	ORNL/TM-2022/2691/V10	Volume 10: Flow Test Facilities
11	ORNL/TM-2022/2691/V11	Volume 11: Modeling & Simulation
12	ORNL/TM-2022/2691/V12	Volume 12: Flow Loop Facilities
13	ORNL/TM-2022/2691/V13	Volume 13: Neutrino Facilities

2.   BACKGROUND

Detailed descriptions of HFIR, the HFIR-SENSe Initiative, and the LEU conversion program are provided in the report by Bryan and Chandler (2023). An overview of HFIR's history, missions, reactor physics performance, and primary systems can be found in the paper by Chandler and Bryan (2021). Section 2.1 of this report provides a brief overview of HFIR and its experiment facilities; the report by Bryan and Chandler can be referred to for more details. Section 2.2 provides an overview of in-core irradiation research with a focus on materials irradiation research.

2.1   DESCRIPTION OF HFIR

HFIR is a versatile, high-performance research reactor that is operated at ORNL on behalf of the DOE-SC. Fueled by HEU and operating at a power level of 85 MW thermal, HFIR typically operates for 23- to 26-day cycles with a 2.5×10^{15} n/cm^2-s peak unperturbed thermal neutron flux, which is the highest in the nation. HFIR's intense neutron flux and state-of-the-art facilities enable world-class capabilities and missions, including cold and thermal neutron scattering, radioisotope production, materials and fuels irradiation research, neutron activation analysis, nonproliferation research, and nuclear physics research. HFIR's multi-mission capabilities are attributed to its high power density core design consisting of a series of concentric regions, each ~24 inches in height, including a flux trap target (FTT), an inner fuel element (IFE), an outer fuel element (OFE), a control element (CE) region, and a large beryllium reflector. Figure 1 shows a HFIR core mockup and description.
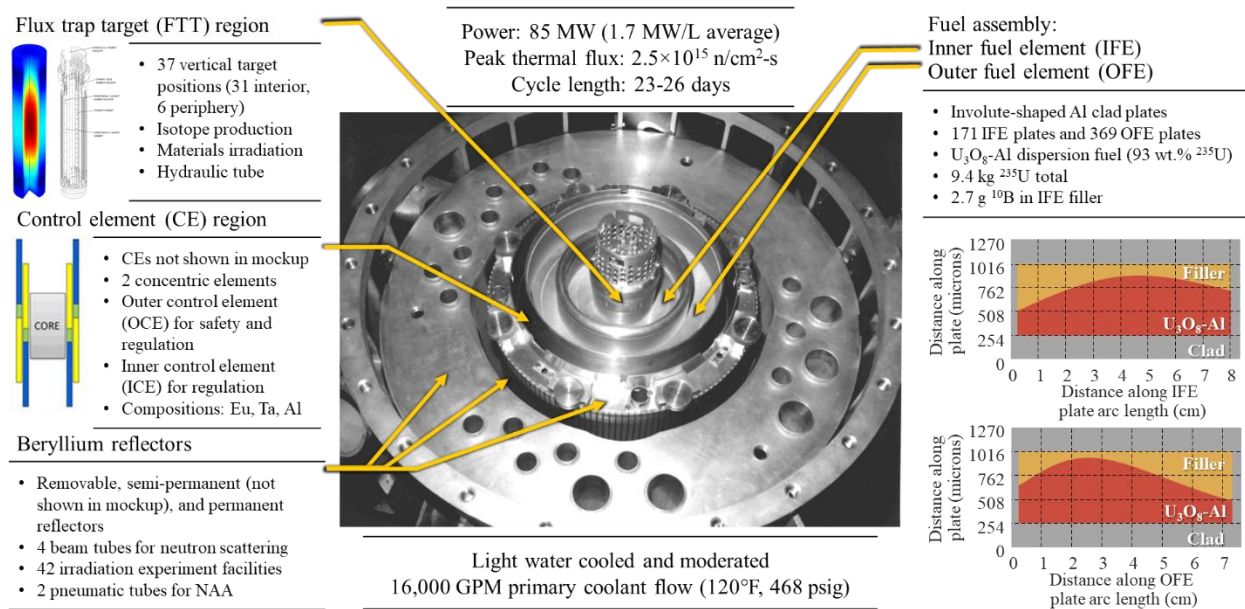
Figure 1. HFIR core mockup and description (Chandler, Bryan, and McDuffee 2022).

The HFIR fuel assembly consists of an integral two element configuration in which the IFE is nested within the OFE. The IFE and OFE contain 171 and 369 involute-shaped fuel plates, respectively, and each Al-clad plate contains a filler and fuel section. The fuel section consists of HEU U$_3$O$_8$ fuel dispersed in an Al matrix. The fuel is enriched to ~93 wt.% ^{235}U, and about 2.6 and 6.8 kg of ^{235}U are loaded into the IFE and OFE, respectively. The filler section is Al; however, the IFE filler section contains ^{10}B burnable poison in the form of B$_4$C homogeneously dispersed in Al. For reactivity control and power regulation, two concentric CEs are in the small water annulus between the fuel assembly and the beryllium reflector. The CEs are axially withdrawn during the cycle by moving the absorber regions away

from the core horizontal midplane to compensate for reactivity changes, which are mostly attributable to fuel and burnable poison depletion and fission product generation.

HFIR was designed with a central, over-moderated FTT region surrounded by the fuel elements because this geometry produces a very high thermal neutron flux in the FTT. A basket-type design provides 37 target positions, including 31 inside the basket, and six around the periphery. Additionally, one of the interior positions includes a hydraulic tube which allows for capsule insertion and removal during the cycle.

The large ring of beryllium reflector is subdivided into three regions, including the removable beryllium (RB), semi-permanent beryllium (SPB), and permanent beryllium (PB) reflectors. The RB, which is closest to the core, houses eight large and four small irradiation facilities. The SPB, located between the RB and PB, is composed of four quadrants separated by control rod access plugs that are each outfitted with two small irradiation facilities (eight in total). The PB is the largest of the three reflector regions and houses 22 vertical experiment facilities (VXFs)—11 inner small, 5 outer small, and 6 outer large facilities—for irradiation experiments and four horizontal beam (HB) tubes for neutron scattering experiments. Additionally, two engineering slant tube facilities (EFs) graze the outer radial edge of the reflector. Two pneumatic tubes, one in the inner small VXF-7 and one in EF-2, are used to shuttle small rabbits in and out of the reactor for neutron activation analysis studies.

2.2   IN-CORE MATERIALS IRRADIATION RESEARCH

ORNL has been one of the leading institutions in the field of radiation materials science (i.e., the effects of irradiation on materials properties) since Eugene Wigner first discussed the possibility of neutrons and gamma rays affecting materials properties (Wigner 1946). The primary focus of radiation materials science is to understand and quantify how the interaction of radiation with solids changes the materials properties and how these changes affect the usable lifetimes of these materials. Even with this 75+ year history of research, the field of radiation materials science is still relatively young, with an almost unlimited range of research opportunities resulting from the development of new materials, novel uses for existing materials, and the objective to extend the current materials usable lifetimes.

The irradiation of materials in HFIR supports programs for DOE, international collaboration, and private industry that range from fundamental radiation effects in materials (DOE-Basic Energy Sciences), fission energy (DOE-Nuclear Energy), fusion energy (DOE-Fusion Energy Sciences), nuclear propulsion (Naval Reactors), neutron production (Spallation Neutron Source second target station), isotope production (SHINE Technologies), and other applications where a material may be exposed to irradiation. Each of these research fields has different needs when it comes to exposing materials to neutron irradiation under representative experimental conditions (i.e., temperature and mechanical loading) that are typical for each material's intended use.

Much of the historical radiation materials science research performed at ORNL has been focused on fundamental understanding of the effects of irradiation on the microstructure and materials properties. Most of these materials irradiations occur within the HFIR FTT, but occasionally, the positions in the RB are utilized for capsules instrumented with thermocouples so that their temperatures are actively controlled by changing the gas mixture that flows through the capsules. The main benefit for performing materials irradiations is that in general, the amount of fast neutron fluence received by these materials in the FTT during typical HFIR operations (5–6 cycles per year) is roughly equivalent to a decade's worth of fluence these materials would receive in a power reactor. More recently, research efforts have begun to include materials irradiations in support of current reactor lifetime extensions and materials development for advanced applications requiring experimental conditions representative of the end use. A primary requirement for supporting such efforts that is not routinely considered is the capability to control either

5

the neutron energy spectrum for materials irradiation or to maintain a constant neutron flux across the material being irradiated. These two needs are the primary drivers for the Spectrum Tailoring Working Group's effort.

An example of the need to control the neutron energy spectrum relates to the study of tungsten as a divertor material for tokamak fusion reactors. When tungsten is irradiated in the HFIR FTT, the transmutation rate per unit of accumulated radiation damage, measured in units of displacements per atom (dpa), is one to two orders of magnitude higher in HFIR relative to a typical fusion system (Figure 2) (Garrison 2019) because of the high neutron flux with neutron energies <100 eV in HFIR (Sawan 2014). The results from unshielded FTT irradiations of tungsten (Katoh 2019) indicate that a transmutation of ~1% (at ~0.1 dpa) results in the approximate end of life for tungsten because of hardening, embrittlement, and weakening of the material. However, the question posed by the research (Katoh 2019) is whether the 1% transmutation lifetime is appropriate for fusion applications, because the transmutation-to-damage ratio would be much smaller in fusion systems. The PHENIX program (Garrison 2019), a United States–Japan collaboration, has been investigating the effect of the reduced transmutation-to-damage ratio on the properties of tungsten. Instead of irradiating tungsten in the HFIR FTT, irradiations occurred in a HFIR RB position. The experiment, referred to as *RB-19J*, was an instrumented experiment during which temperature was actively monitored with thermocouples and controlled by adjusting the gas mixture flowing through the experiment. The RB-19J capsule included a Gd shield that preferentially absorbs thermal neutrons to reduce the transmutation-to-damage ratio (shown as the green circle in Figure 2) to a level predicted for fusion systems. The early results from the RB-19J experiment do not show any significant difference between the hardening of single crystal tungsten irradiated in unshielded flux trap capsules (~5% transmutation, ~0.4 dpa) and the hardening of single crystal tungsten in the shielded RB-19J (~0.2% transmutation, ~0.8 dpa) (Garrison 2019). Further investigations may show that the 1% transmutation limit may still be the effective end of life for tungsten in fusion systems, but the 1% limit would translate to a total damage of 1–10 dpa in a fusion-typical neutron spectrum rather than the 0.1 dpa that occurred from irradiation in the softer neutron spectrum in the unshielded HFIR FTT experiment capsules. In summary, spectrum tailoring is needed to reduce the thermal neutron flux in HFIR irradiation facilities to reduce material transmutation in materials irradiation specimens.
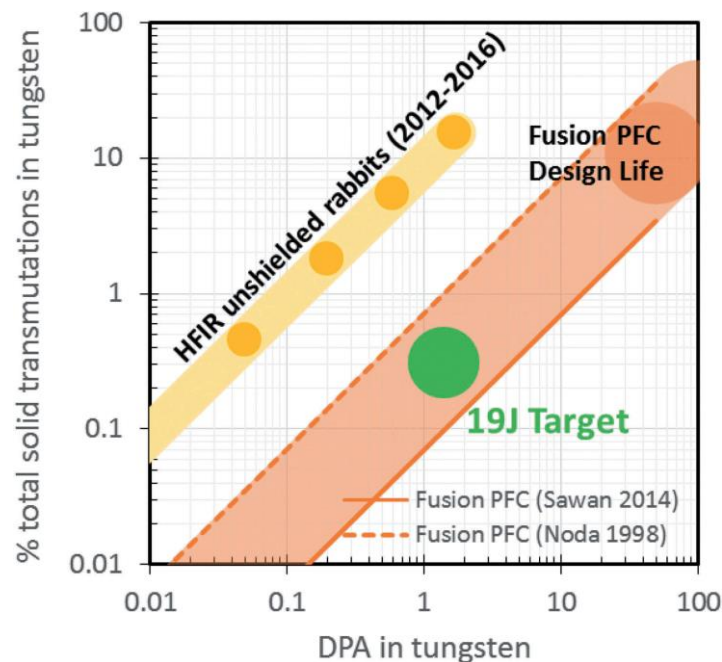
Figure 2. Predicted tungsten transmutation in unshielded HFIR flux trap capsules (yellow) and expected fusion reactor neutron spectrum (Garrison 2019).

Other needs related to controlling the neutron energy spectrum arise from both fission and fusion reactor applications. Several next-generation reactors under development are fast-spectrum systems such as the traveling wave reactor being developed by TerraPower. Like fusion reactors, these fast-spectrum systems have different materials property changes compared to those that occur in a thermal reactor energy spectrum (i.e., light-water reactors). One primary change that requires study is helium embrittlement of nickel-based alloys in fast reactors (Griffiths 2020) and ferritic-martensitic (FM) steels in fusion reactors (Hashimoto 2020). Tailoring HFIR's neutron spectrum for fast fission reactor testing could be accomplished with the use of thermal neutron shielding (e.g., Eu_2O_3 or Gd). Obtaining fusion-typical spectrums is not as likely in HFIR because of the lack of neutrons at the >10 MeV range energy present in deuterium–tritium (D-T) fusion systems that cause the helium embrittlement. This obstacle has been approached in the past by doping FM steels with either [10]B or [58]Ni, increasing the isotopic content of [54]Fe, pre-irradiation helium implantation, or performing high-energy proton irradiation at spallation neutron sources (Hashimoto 2020). Doping with [10]B or [58]Ni is less than ideal because the dopants affect the as-manufactured microstructure and mechanical properties. The [54]Fe isotopic adjustment can be cost prohibitive, and helium implantation can alter the helium distribution that would develop in a fusion system. Also, the spallation exposures resulted in transmutation elements from the proton interactions that would not be present in fusion systems (Hashimoto 2020).

The other need for spectrum tailoring is to have a spatially uniform neutron flux across a material being irradiated for materials qualification testing. High-temperature reactor designs are focused on using ceramic matrix composites (CMCs)—typically carbon-carbon (C/C) or silicon carbide / silicon carbide (SiC/SiC). These components must undergo qualification testing according to specifications established in the American Society of Mechanical Engineers (ASME) Boiler and Pressure Vessel Code, Section III, Division 5, High Temperature Reactors (ASME 2021). In this code, article HHB-III-4000, Requirement for Representative Data, specifies that the effects of irradiation on the CMC material properties shall be obtained from representative material and that it is up to the designer to justify what qualifies as "representative data." Part of the reason for this ambiguity is that the various CMC shapes to be used are dependent on the end use (e.g., supports, restraint straps, control rod sleeves, hangers). Different shapes also use different fiber architectures, which can dramatically alter the CMC properties and responses to irradiation. For this reason, it is likely that at least part of a CMC qualification testing program will require irradiation of CMCs of the same shape, dimensions, and fiber architecture as the final components. An example of a potential CMC component would be a C/C control rod sleeve (arbitrary dimensions/configuration) with a 50 mm outer diameter (OD) cylinder, a 3 mm wall thickness, and a fiber weave with a 60-degree braiding around the cylinder. A piece of this hypothetical C/C control rod sleeve would require irradiation out in the PB region either in the small or large VXF positions. However, when performing materials irradiation in these positions, the fast neutron flux decreases by a factor of 1.7–2.7 radially. Even the RB positions experience a fast-flux decrease by a factor of 2.4 radially across the position. The change of core horizontal midplane fast neutron flux in the reflector is plotted vs. distance from reactor core centerline in Figure 3. The vertical dashed lines indicate the radial distances from the core centerline to the inner and outer radii of the various experimental locations. This difference in flux across the hypothetical control rod sleeve would result in a nonuniform dimensional change of both the fiber and the matrix which could result in the buildup of internal stresses that would fundamentally alter the material property changes caused by irradiation. This could prove to be a problem if this hypothetical control rod sleeve is expected to have a uniform neutron flux in the cross section when in operation. Therefore, it is necessary to investigate possible spectrum tailoring options that could assist with flattening the fast neutron flux across the larger irradiation positions in the RB and PB positions.
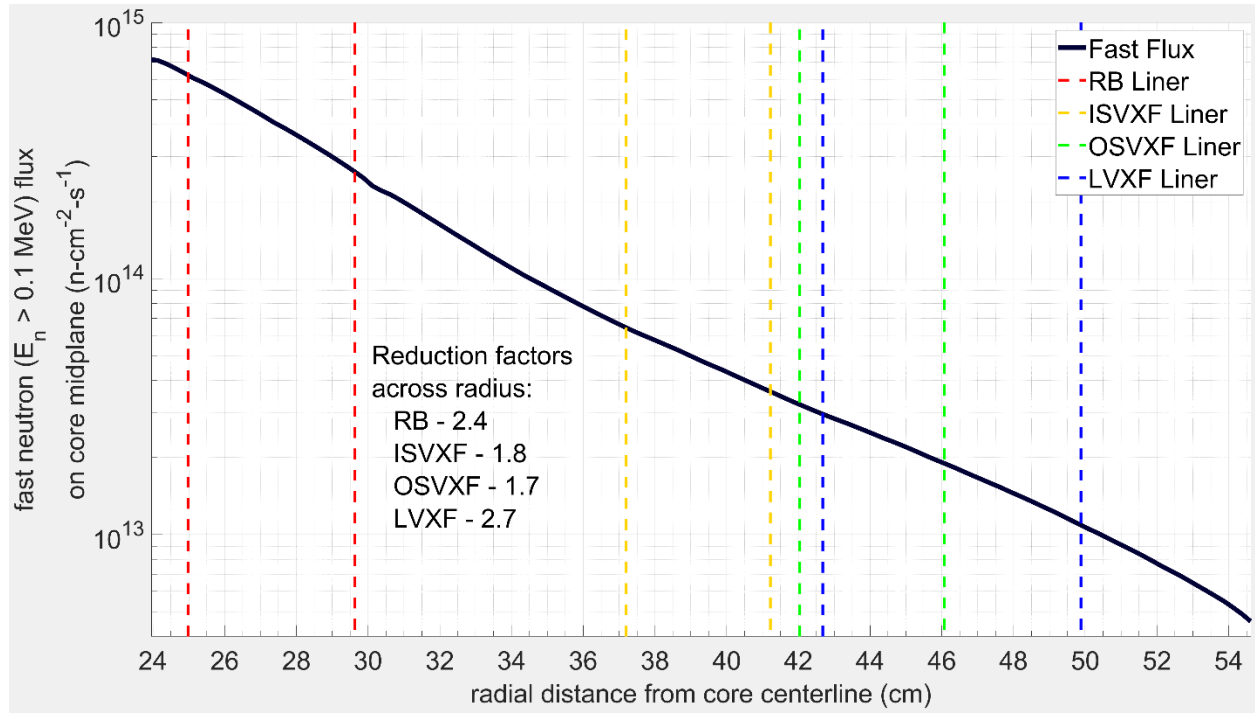
Figure 3. Plot of midplane fast neutron flux vs. radial distance from HFIR centerline in the reflector. Vertical dashed lines indicate the radial locations of the four different reflector irradiation positions.

3. WORKING GROUP OBJECTIVES AND GOALS

A technically diverse group of ORNL irradiation experiment subject matter experts form the Spectrum Tailoring Working Group, as shown in Table 2. The goal of the working group is to develop a compendium of concepts to enhance in-core irradiation experiment conditions via neutron energy spectrum tailoring, resulting in increased high-impact science at HFIR. The significance of this working group is described in Section 2.2.

Table 2. Spectrum Tailoring Working Group team members

Member	Division	Group
David Chandler	Nuclear Energy and Fuel Cycle	Research and Test Reactor Physics
Anne Campbell	Materials Science and Technology	Nuclear Energy Materials Microanalysis
Charles Daily	Nuclear Energy and Fuel Cycle	Radiation Transport
Jianwei Hu	Nuclear Energy and Fuel Cycle	Research and Test Reactor Physics
Zain Karriem	Radioisotope Science and Technology	Target Design, Analysis, and Qualification
Jeff Powers	Nuclear Energy and Fuel Cycle	Advanced Reactor Systems
Yanwen Zhang	Materials Science and Technology	Radiation Effects and Microstructural Analysis

The working group held routine meetings approximately every two weeks between November 2021 and March 2022 to brainstorm concepts and to discuss the information documented in this report. The purpose of this report is to document the efforts accomplished in FY22 regarding
1. developing the concepts,
2. building scientific justifications for the various concepts,
3. identifying potential facility sponsors, and
4. estimating costs and schedules for each concept.

These items may be developed further in FY23 or beyond based on the future direction of the HFIR-SENSe Initiative and the interest of potential sponsors.

4. SPECTRUM TAILORING PRECONCEPTUAL DESIGN DEVELOPMENT

The working group discussed and evaluated several ideas to improve spectrum tailoring capabilities in HFIR's beryllium reflector experiment facilities. Four primary objectives of a spectrum tailoring experiment facility were identified:
1. ability to significantly reduce the thermal neutron flux to the experiment
2. ability to increase the fast neutron flux to the experiment for increased damage rates (i.e., dpa)
3. ability to modify the full neutron energy spectrum to better mimic user-desired conditions (e.g., PWR, advanced reactors, fission reactors)
4. ability to flatten the neutron flux profile across the experiment

The concepts recommended for further analysis have been divided into three categories and are discussed in detail in Sections 4.1–4.3. Section 4.1 documents preconceptual designs focused on experiment facility configuration improvements within the current beryllium reflector irradiation holes. Beryllium reflector design changes capable of enhancing materials / fuels irradiation research and spectrum tailoring are discussed in Section 4.2. A new, innovative ion beam facility is conceptualized in Section 4.3 that would enable combined neutron/ion and separate effects testing to enhance materials irradiation research.

The goals of this Spectrum Tailoring Working Group are synergistic with those of several other HFIR-SCIENCE and HFIR-CRITICAL working groups. The Flexible Flux Trap Working Group is exploring preconceptual designs to enhance the flexibility of the flux trap for irradiation experiments and thus the Spectrum Tailoring Working Group focused on the beryllium reflector irradiation facilities. Additionally, the Flow Loops Working Group is discussing various flow loop options, which is one reason that flowing moderators and poisons were not pursued in the Spectrum Tailoring Working Group. Furthermore, preconceptual designs discussed for spectrum tailoring that impact the beryllium reflector design will be communicated to HFIR-CRITICAL's Reflector Design Working Group for further consideration.

4.1 EXPERIMENT FACILITY FILTERS AND BOOSTERS

The experiment facility filter and booster preconceptual design ideas utilize existing reflector facilities such as the large RB facilities that can be instrumented or uninstrumented. This group of design ideas does not modify the reactor configuration or introduce a new system, and it builds on lessons learned from previous experiments that utilized thermal filters. Such experiments are very costly and may not be optimized because of time and funding constraints. Designing and optimizing spectrum tailoring components such as those described below to meet HFIR safety basis requirements would significantly enhance experiments requiring spectrum tailoring while also reducing experiment design and analysis time and costs. The experiment facility preconceptual filter and booster designs are summarized in Table 3.

Several possibilities exist to accomplish the four primary objectives defined above to improve spectrum tailoring capabilities. Nonthermal neutrons leak out of the fuel assembly into the flux trap and beryllium reflector regions where they are moderated to slower energies as a result of interactions with the water moderator / coolant and the beryllium reflector. Modification of materials between the fuel assembly and the subject experiments is the most practical means for achieving an increased fast flux and a reduced thermal flux at the experiment site. Because HFIR is a light-water cooled and moderated reactor, reducing / removing water surrounding the fuel and control elements is not feasible. However, manipulation of the materials surrounding the experiment is feasible and may be the best approach for tailoring the spectrum.

General possibilities to reduce the thermal neutron flux to irradiation facilities include removing / reducing the amount of moderating material around the facility, surrounding the experiment with a
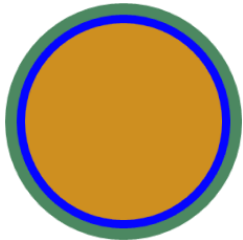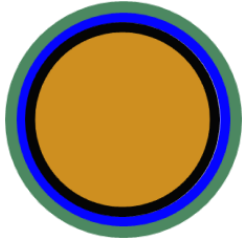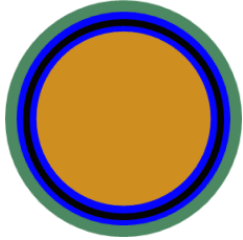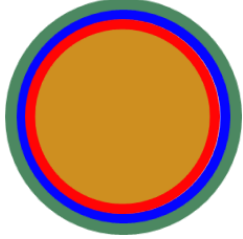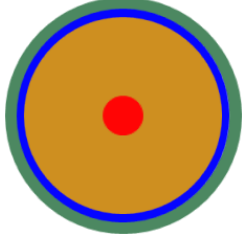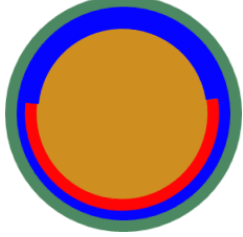
thermal neutron filter, and placing a fueled fast-flux booster around the experiment. Reducing the amount of moderating material around the facility, such as water and beryllium, will reduce the number of neutrons being slowed down from nonthermal energies, thereby reducing the thermal flux. Thermal filters (e.g., Eu, Gd, Hf, Sm) with high thermal neutron absorption cross sections around the experiment will absorb a large fraction of the thermal neutrons that would otherwise interact with the experiment. Lastly, a fueled (e.g., U, Pu) fast-flux booster would contain elements with high thermal absorption cross sections, thus leading to a reduced thermal flux to the experiment.

General possibilities to increase the fast neutron flux to irradiation facilities are similar to those previously described to reduce the thermal neutron flux. Less fast neutrons are slowed down to thermal neutrons by reducing the moderating material between the fuel and the experiment, thereby increasing the fast flux. Fast neutron flux boosters can absorb non-fast neutrons and produce fast neutrons via fission, thereby increasing the fast flux. Additionally, irradiation facilities in the beryllium reflector could be moved closer to the fuel assembly to achieve increased fast fluxes.

Using a combination of flux filters and boosters is the most practical way to tailor the neutron energy spectrum, an approach which may be important to certain experiments. For example, if an advanced reactor material or fuel is to be irradiated in a prototypic neutron spectrum, then a combination of filters and boosters could make this possible. Thermal and resonance filters could be used to reduce neutrons in the thermal and resonance energy regions, respectively, and fast-flux boosters could be used to increase the high-energy neutron flux.

The ability to flatten the fast neutron flux gradient across experiments in the beryllium reflector is also important, as discussed above. Experiment facilities in the reflector experience large fast-flux gradients from the front side to the back side because the neutron source (i.e., the fuel assembly) is closer to the front side of the facility. One means to achieve a flatter flux includes placing a fast-flux booster on the back side of the experiment, thus introducing a fast neutron source behind the experiment.

Table 3. Summary of experiment facility preconceptual filter and booster designs

Design concept description	Design concept illustration
0. A typical HFIR beryllium reflector facility consists of an Al liner with an experiment inside. Unused facilities, depending on location, contain a Be plug, Al plug, or water with a stainless steel inner liner / flow orifice.	
1. An annular thermal or resonance filter surrounding a materials or fuels irradiation experiment will significantly reduce the thermal or resonance neutron flux to the experiment. These filters will tailor the neutron flux spectrum.	
2. Replaceable Al liners—with an option to include thermal and/or resonance filters inside the liner—will perform a function similar to that of design 1 but will increase the available volume for the experiment relative to design 1.	
3. An annular fast-flux booster outside of the materials or fuels irradiation experiment will simultaneously reduce the non-fast neutron flux and will increase the fast neutron flux.	
4. The flux booster inside the experiment will result in an increased fast flux and may help to flatten the fast-flux profile across the experiment.	
5. A partial annular (i.e., semi-circle) fast-flux booster on the backside of the facility will flatten the fast neutron flux profile across the facility.	

⬤ beryllium reflector ⬤ aluminum liner ⬤ experiment ⬤ thermal or resonance filter ⬤ fast flux booster
(water coolant channels not depicted)

The design concepts illustrated in Table 3 can be used across a range of combinations to achieve a variety of neutron flux distribution modifications. Some example configurations of neutron filters and fueled fast neutron flux boosters are provided in Table 4. As indicated, many potential combinations exist, and they can be grouped into four generic categories:

a. designs tailoring the non-fast neutron flux only (concepts 1 and 2),
b. designs significantly enhancing the fast neutron flux and reducing the non-fast neutron flux (concepts 3–5),
c. designs significantly increasing the fast neutron flux and significantly decreasing the thermal neutron flux (concepts 1–5), and
d. designs significantly altering the entire neutron energy spectrum.

Table 4. Experiment facility filter and booster design configuration examples

Design configuration description	Design configuration illustration
1. Thermal and / or resonance filter (concept 1 or 2) combined with an outer fast-flux booster (concept 3) will increase the fast neutron flux and significantly reduce the non-fast neutron flux.	
2. Thermal and/or resonance filter (concept 1 or 2) combined with an inner fast-flux booster (concept 4) will increase the fast neutron flux and significantly reduce the non-fast neutron flux.	
3. A partial annular (concept 5) fast-flux booster on the backside of the facility with a thermal and/or resonance filter outside of the experiment (concept 1 or 2) will flatten the fast neutron flux profile across the facility and reduce the non-fast neutron flux. Note: The booster must be outside the filter to increase booster efficiency.	
4. A partial annular (concept 5) fast-flux booster on the backside of the facility with an inner fast-flux booster (concept 4) and a thermal and / or resonance filter outside the experiment (concept 1 or 2) will increase the fast neutron flux, flatten the fast neutron flux profile across the facility, and reduce the non-fast neutron flux.	

⊙ beryllium reflector   ⊙ aluminum liner   ● experiment   ⊙ thermal or resonance filter   ⊙ fast flux booster
(water coolant channels not depicted)

4.1.1   Design Requirements

The spectrum tailoring facility should meet all requirements discussed in the Safety Analysis Report (SAR), Technical Safety Requirements (TSRs), and Experiment Guides (EGs). Per EG 1 (EG-1) and Chapter 10 of the SAR, all in-vessel experiments must be reviewed and approved to ensure that the experiment:

- poses no unacceptable risk to the safety of the reactor or personnel,
- poses no unreviewed safety question,
- is in compliance with applicable TSRs,
- does not adversely affect the predictability or availability of reactor operations, and
- does not adversely affect key research programs that fund the reactor.

The intent of the spectrum tailoring preconceptual designs is to modify the neutron spectrum to experiment facilities. Modifications include depressing the thermal neutron flux and increasing and flattening the profile of the fast neutron flux. Introduction of poison materials (e.g., Eu, Sm, Gd, Hf) near the fuel assembly tends to locally depress the power densities in the fuel, which results in power increases elsewhere. Poison materials also reduce the core reactivity worth and therefore impact the startup symmetrical critical control element position and the cycle length. Fueled fast-flux boosting targets also can perturb the fuel assembly power distribution and core criticality. The spectrum tailoring facility components will fit inside a beryllium reflector experiment facility hole and should be latched down (e.g., hold-down yoke) to prevent the possibility of ejection during operation, which could cause a reactivity insertion accident.

The effect of all experiments in the flux trap and Be reflector, including the spectrum tailoring facility, must not perturb the power distribution within the fuel assembly that could result in less conservative set point values. The experiment configuration must not result in an increased power density (i.e., flux tilt) greater than or equal to 9%. A cycle length reduction caused by a negative reactivity insertion does not necessarily adversely affect nuclear safety, but it does affect the ability to carry out key research missions such as neutron scattering. Division director approval must be granted for experiments expected to reduce the cycle length, and cycle length penalty reduction fees may be incurred. If the cycle reduction is expected to be greater than 1.3 days, then associate lab director (ALD) approval must be requested. The experiment configuration must not perturb the neutron current down any of the four beam tubes by more than 5%. However, if a perturbation greater than 5% is expected, then ALD approval must be requested. Thus, the spectrum tailoring facility should:
- not result in a flux tilt greater than 9%,
- not result in a cycle length reduction greater than 1.3 days, or
- not result in a neutron current reduction down any beam tube greater than 5%.

Heat deposition rates in neutron filters and fueled targets are high, especially in high neutron and gamma flux environments. The heat deposited in all spectrum tailoring facility components must be dissipated by adequate coolant flow. Under normal full-power operating conditions, the surface temperature of the poison filter and fueled flux booster cladding (and other components in contact with water coolant) shall not exceed the saturation temperature of the reactor to avoid possible burnout or steam blanketing. All reactivity, thermal, hydraulic, and structural requirements defined in the SAR (Chapter 10 addresses experiments), TSRs, and the EGs must be met. EG-6 provides a standardized means for performing and documenting the safety and operability reviews required for in-vessel irradiations.

4.1.2 Limitations/Challenges

Fast-flux boosting targets will contain fuel such as ^{235}U, so the target would impose special storage, security, and / or monitoring requirements. Depending on the amount of fuel in the proposed booster target(s), the target may adversely affect the source term, nuclear criticality evaluation, or other factors. These effects must be evaluated in detail prior to experiment insertion.

The concepts should be designed to be multi-purpose, generic, and standard to reduce design and analysis times, experiment costs, and associated risks. With a long list of spectrum tailoring possibilities,

optimization of the various concepts may be difficult because the performance requirements may be experiment- and user-specific.

4.1.3 Calculations

Scoping calculations were performed to gain a better understanding of the impacts that various fast-flux boosters and neutron filters have on neutron fluxes in experiments in the RB facilities and the PB VXFs. No efforts were made to optimize the configurations in these scoping efforts. The Monte Carlo N-Particle (MCNP) code (X-5 2003) and the end-of-cycle (EOC) PB reflector number 5 model (Chandler and Navarro 2022), which is based on the homogenous, representative core model (Chandler 2020), were used in this study. An illustration of the base model with Be plugs in all removable and permanent reflector experiment facilities except the pneumatic facility in VXF-13 is provided in Figure 4.
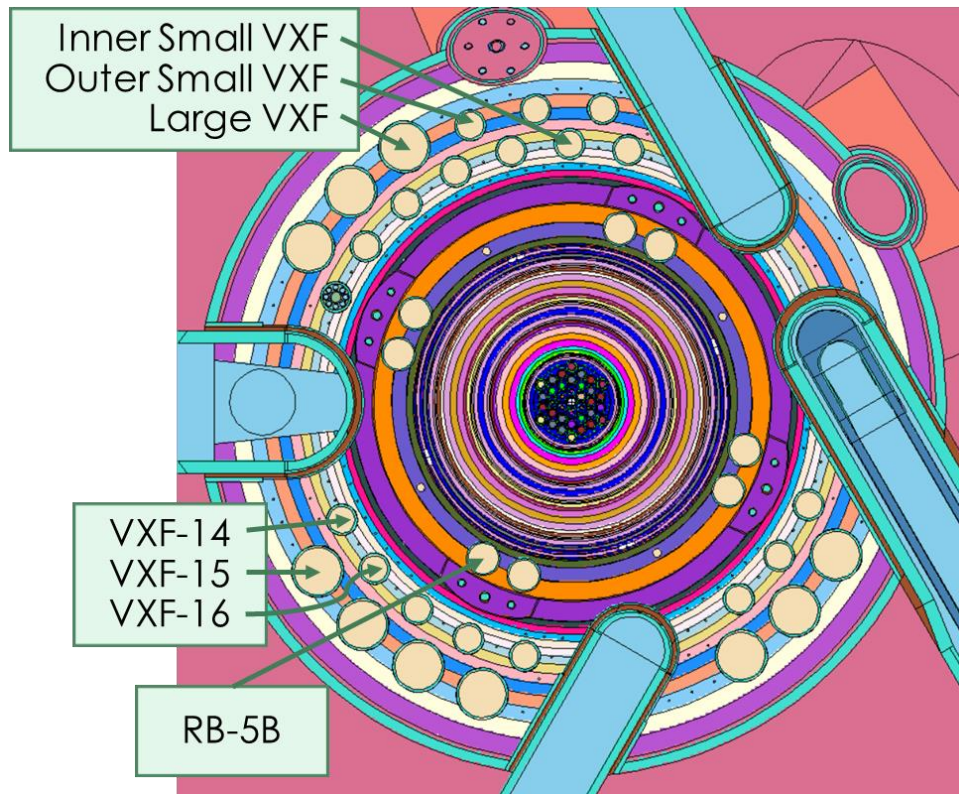
**Figure 4. Cross section of the HFIR PB reflector number 5
MCNP model on the core horizontal midplane.**

To understand the neutron spectrum in the reflector facilities and identify neutron filter isotopes, the neutron flux in a 44-energy group structure and a 3-energy group structure was tallied in the aluminum liners of the reflector, over its entire length of 60.96 cm. Additionally, the three-energy group capture cross sections for all isotopes found in the ENDF/B-VII.0 cross section library (Chadwick 2006) were tallied. The cross sections were calculated primarily to determine isotopes / elements having promise for use as thermal and resonance filters. The neutron flux profiles and the RB liner-based isotopic cross sections are illustrated in Figure 5 and Figure 6, respectively. The cross sections calculated in the other liners vary by less than a factor of 2 for all isotopes relative to the RB liner-based results; however, the results are visually similar given the range of the y-axis in Figure 6. Isotopes of Sm, Eu, Gd, and Hf are identified in Figure 6 because these elements are often utilized as neutron poisons in the nuclear industry for their neutron capture capabilities.
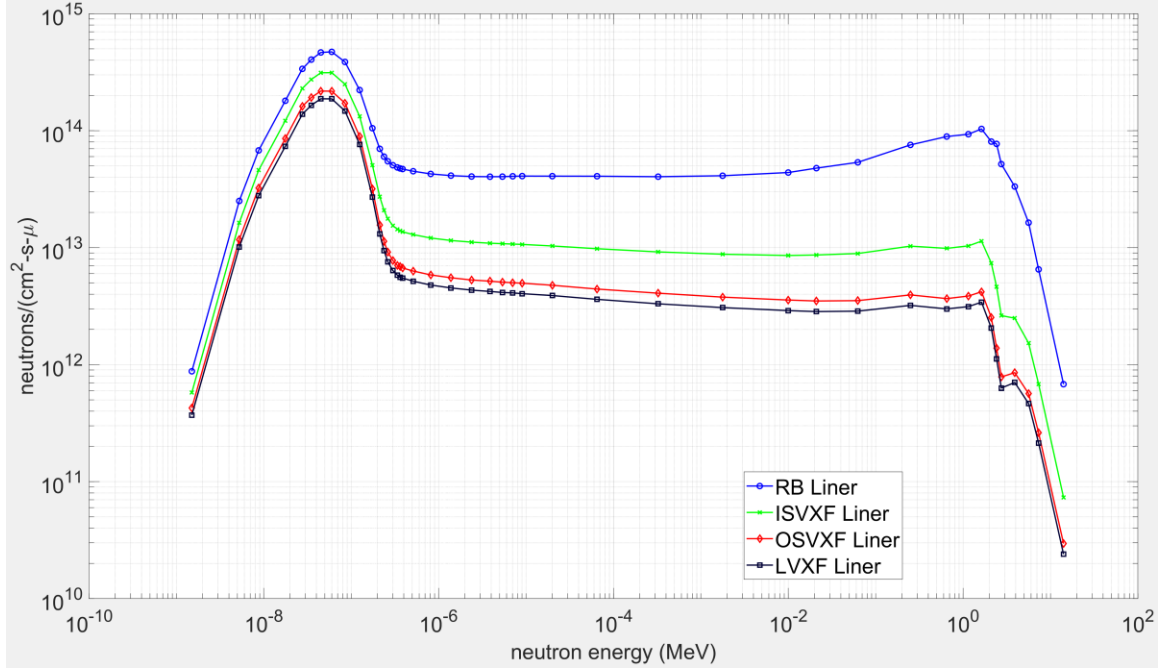
Figure 5. Neutron flux per unit lethargy spectrum calculated in Be facility aluminum liners.
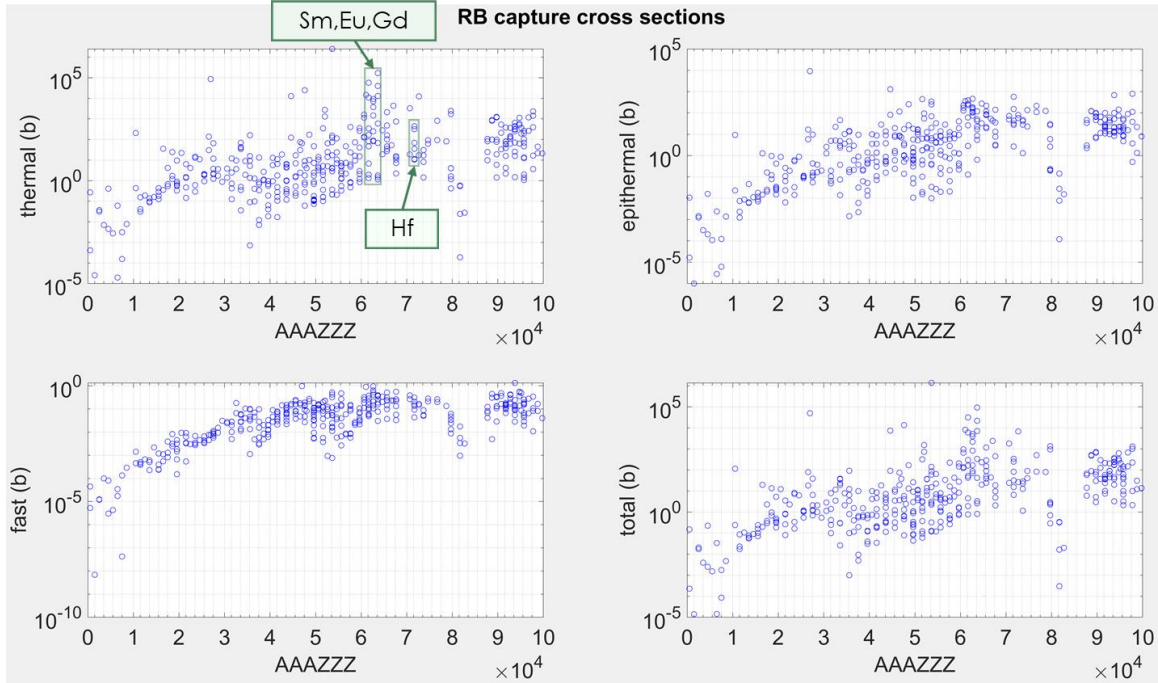
Figure 6. Three-energy group and total isotopic capture cross sections based on RB liner flux spectrum.

4.1.3.1   RB reflector calculations

The peak EOC fast neutron flux on the RB centerline / midplane in a Be plug is about 4.1×10^{14}, and it is about 4.4×10^{14} n-cm^{-2}-s^{-1} in an aluminum plug. The RB-5B facility (Figure 4) was selected for use in a perturbation study to evaluate some of the concepts discussed in Table 3 and Table 4. A total of 14

16

configurations were modeled and are visually provided and listed in Figure 7 and Table 5. When no experiment is loaded in an RB facility, it is loaded with a Be plug to increase core reactivity. Therefore, this configuration should be considered the reference configuration when evaluating core reactivity. For this scoping study, the simulated experiment is an aluminum plug, so the aluminum plug case is considered the reference case when evaluating flux distributions inside the experiment.

Additionally, four configurations modeling poison filters were developed as illustrated in the bottom left case shown in Figure 7. The Gd, Eu, Sm, and Hf poison liners were assumed to be 0.1 cm thick based on the RB-19J experiment configuration calculations (Daily 2016). Four cases were executed with annular flux boosters surrounding a 0.1 cm thick Gd poison filter (top right case shown in Figure 7). The fast-flux booster targets were assumed to be 0.38 mm (15 mils) thick and were in the form of LEU U-10Mo monolithic foils with enrichments of 5, 10, 15, or 19.75 wt.% ^{235}U. Lastly, four semicircle fast-flux boosters surrounding a Gd poison filter were analyzed as shown in the bottom right case in Figure 7.
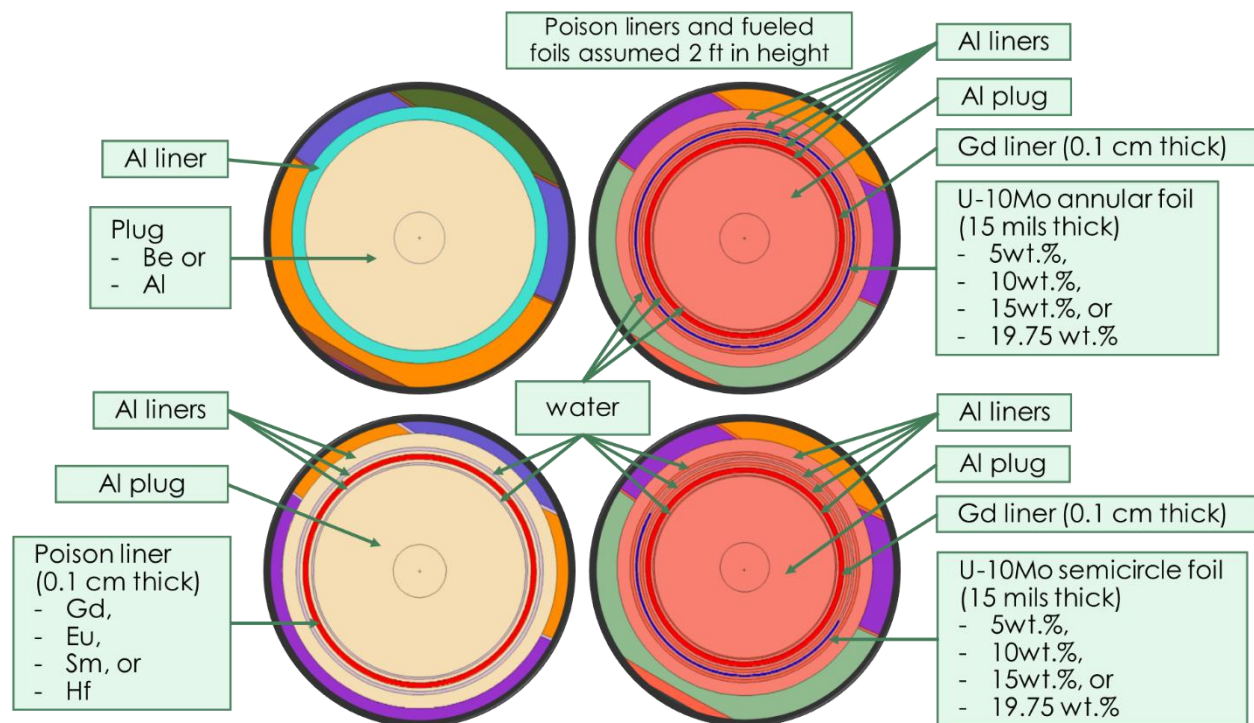
Figure 7. RB-5B experiment facility configurations evaluated.

The calculated eigenvalues (i.e., k$_{eff}$) for the analyzed cases are provided in Table 5. These calculations were performed under EOC conditions when the control elements are fully withdrawn because when the control elements withdraw during the cycle, the neutron source to the reflector increases. Therefore, the reactivity worths reported in this table are considered limiting results and are greater than they would be if calculated under beginning-of-cycle conditions. The worth of changing the Be plug to an aluminum plug is -21¢. The worth of the four poison filters varies between -88¢ and -104¢, and adding fast-flux booster targets (full annular or semicircle) around the Gd poison filters reduces the negative reactivity impact: the worth of the combined filter and booster configurations varies between -43¢ and -84¢.

Table 5. Reactivity worth (ρ) impact of RB-5B experiment facility configuration under EOC conditions

Case	Poison filter	Flux booster	k_{eff}	Unc.	ρ (pcm)	σ_ρ (pcm)	ρ (¢)	σ_ρ (¢)
Be plug	-	-	1.00308	0.00004	-	-	-	-
Al plug	-	-	1.00152	0.00004	-155	6	-21	1
Gd filter	Gd	-	0.99626	0.00004	-682	6	-93	1
Eu filter	Eu	-	0.99547	0.00004	-762	6	-104	1
Sm filter	Sm	-	0.99608	0.00004	-701	6	-95	1
Hf filter	Hf	-	0.99664	0.00004	-644	6	-88	1
5.00 wt% annular	Gd	U-10Mo	0.99753	0.00004	-555	6	-76	1
10.00 wt% annular	Gd	U-10Mo	0.99848	0.00004	-459	6	-63	1
15.00 wt% annular	Gd	U-10Mo	0.99915	0.00004	-392	6	-53	1
19.75 wt% annular	Gd	U-10Mo	0.99989	0.00004	-318	6	-43	1
5.00 wt% semicircle	Gd	U-10Mo	0.99694	0.00004	-614	6	-84	1
10.00 wt% semicircle	Gd	U-10Mo	0.99742	0.00004	-566	6	-77	1
15.00 wt% semicircle	Gd	U-10Mo	0.99777	0.00004	-531	6	-72	1
19.75 wt% semicircle	Gd	U-10Mo	0.99804	0.00004	-503	6	-69	1

The neutron flux in a 44-energy group structure and a 3-energy group structure was tallied in a small tally cylinder modeled at the centerline / midplane of the RB-5B facility in the aluminum plug simulating an experiment. The 44-energy group flux profiles are provided in Figure 8. Despite simulating 500 million active particles, the statistics associated with the low-energy flux bins are high / poor as a result of the effectiveness of the poison filters. However, the statistical uncertainties accompanying the 3-energy group fluxes presented in Figure 9 are low. Depletion calculations were not performed in this scoping calculation to evaluate the impact of transmutation on time-dependent reactivity and flux depression effects.
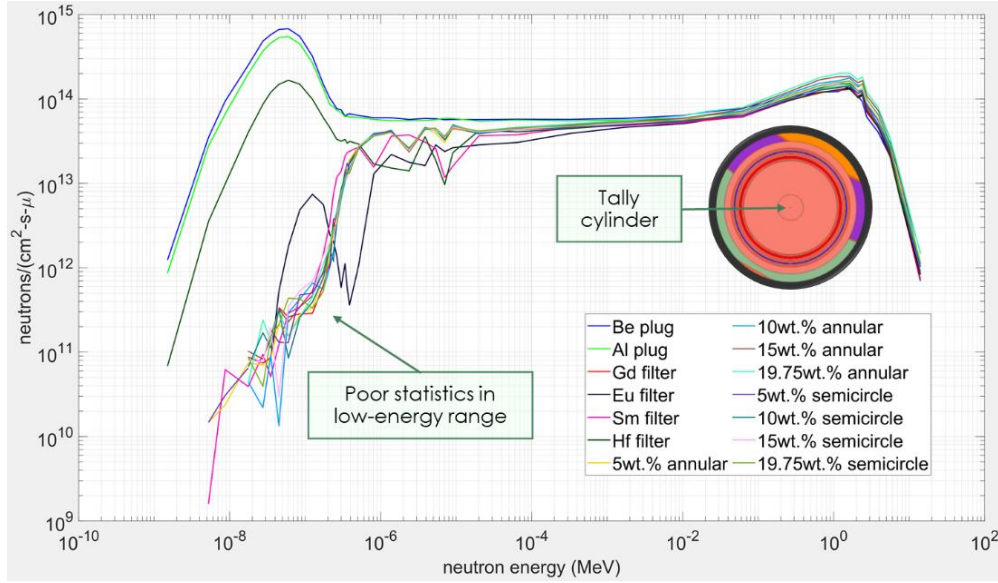
**Figure 8. 44-energy group neutron flux per lethargy profiles
in the tally cylinder for the RB-5B configurations.**

As shown in Figure 8 and Figure 9, the Eu poison filter results in the greatest reduction to the thermal flux (factor of 132 reduction relative to aluminum plug case), followed by the Gd and Sm filters. The Hf filter is the least effective of the four filters analyzed. As expected, the fully annular 19.75 wt% enriched results in the greatest fast neutron flux, which is about 34% greater than the reference aluminum plug case. Although 34% may not seem to be too great of an increase, this could notably reduce the number of required irradiation cycles to 3 instead of 4, for example.
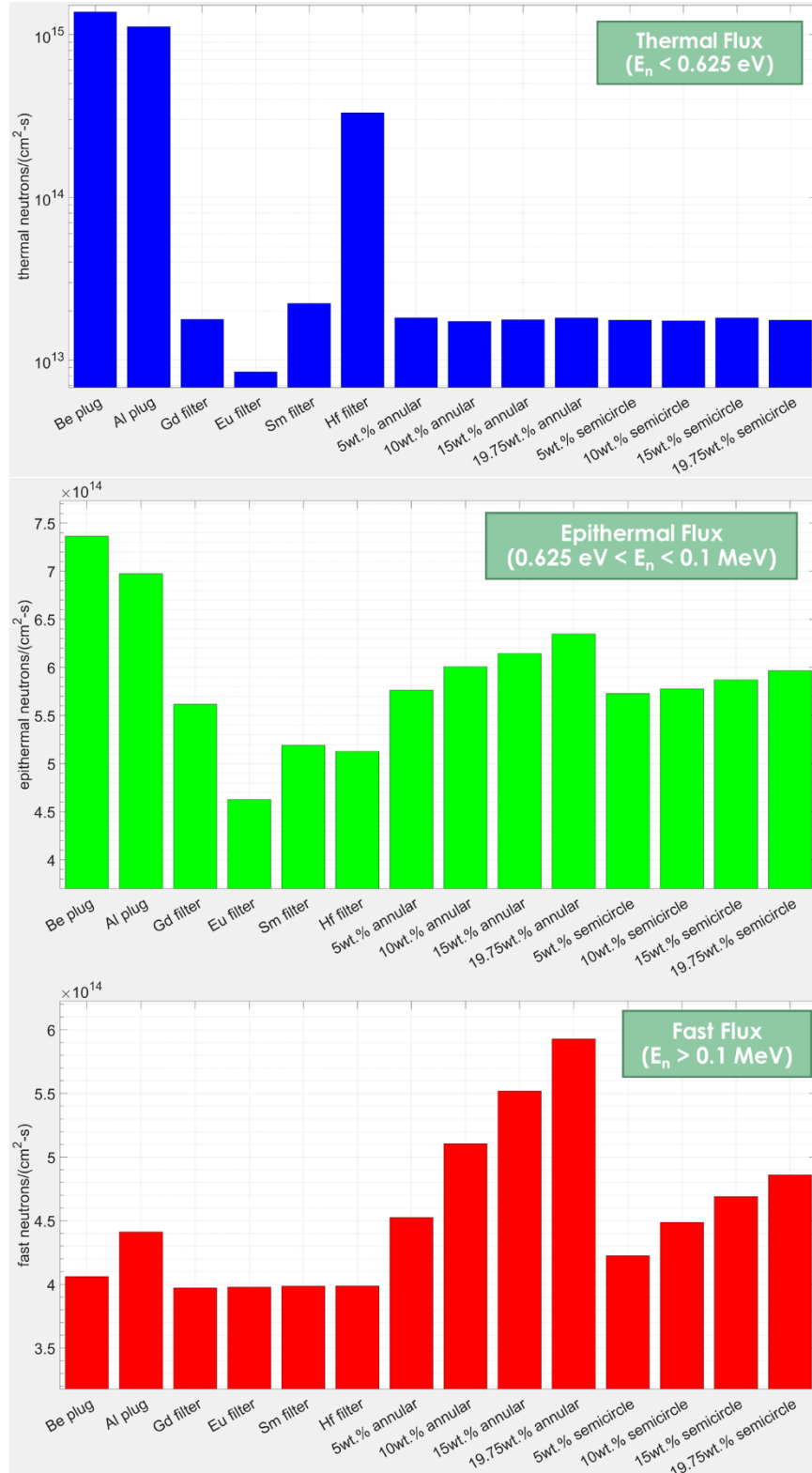
Figure 9. Three-energy group neutron fluxes for the RB-5B experiment facility configurations.

The three-energy group neutron flux r-θ distribution on the core midplane in the RB-5B facility was also tallied for the 14 configurations analyzed. The outer radius of the mesh superimposed on the geometry is 2.60 cm, which is just radially outward to the aluminum liner. An eight radial (0.325 cm Δr) by 12 azimuthal (30° Δθ) mesh was defined. As described in Section 2.2 and further concluded in the beryllium plug case calculation, the fast neutron flux reduces by greater than a factor of 2 across the RB facility. The fast neutron flux reduces by about 40% for the aluminum plug case when considering the plug positioned inside the liner.

Figure 10 illustrates the Gd poison filter case's flux distributions and its results relative to the reference aluminum plug case. Relative to the reference case, the centerline thermal flux is reduced by a factor of 63, and the centerline fast neutron flux is reduced by about 10%. Figure 11 and Figure 12 respectively illustrate the distributions for the 19.75 wt% annular and semi-circle flux booster cases with Gd poison filters. Introduction of the annular fast-flux booster increases the experiment's fast flux, and the fast-flux gradient across the facility is reduced to about 30–35%. The fast-flux gain with the semi-circle booster is not as great as the fully annular booster; however, the fast-flux gradient across the facility is further reduced to less than 20%. Similar plots for the other configurations are provided in Appendix A.
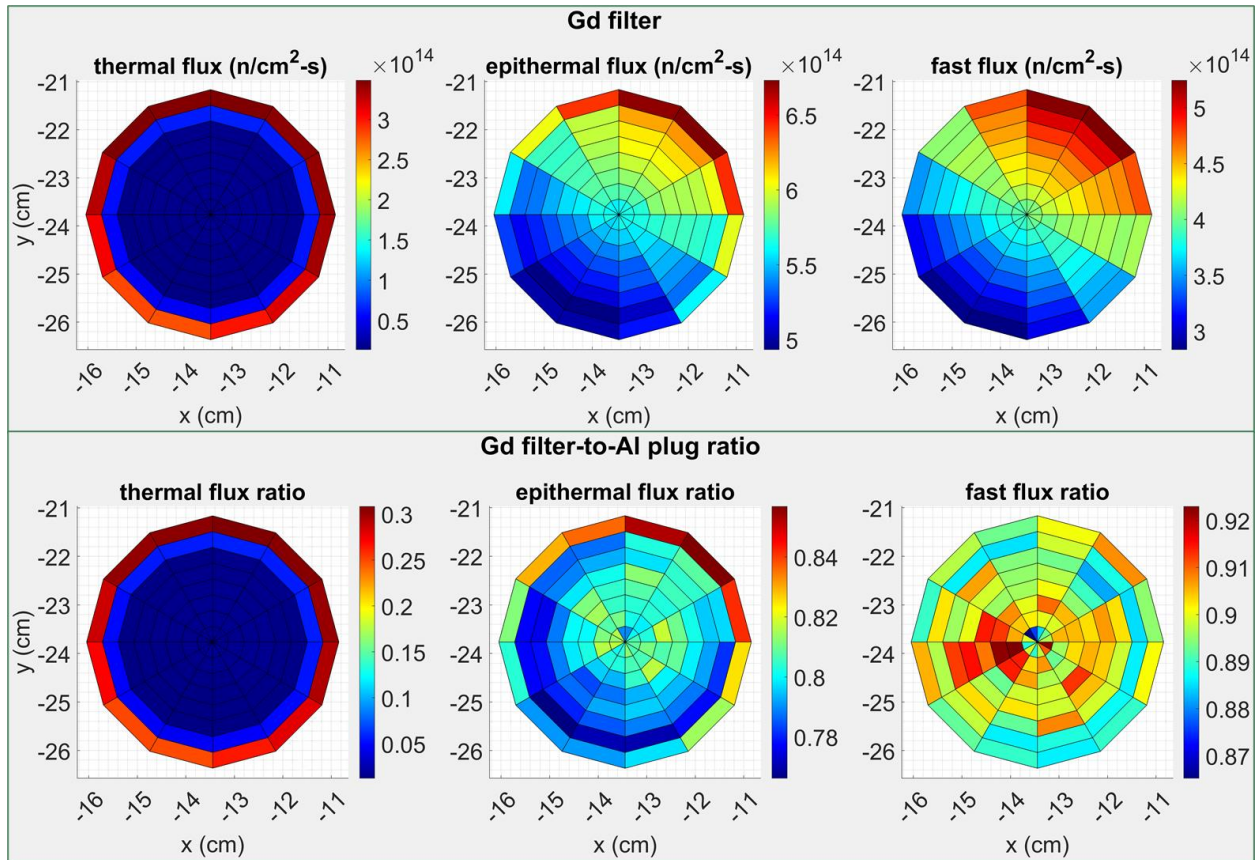
Figure 10. Three-energy group neutron flux distribution in the Gd poison filter configuration and comparison to the reference Al plug case.

21
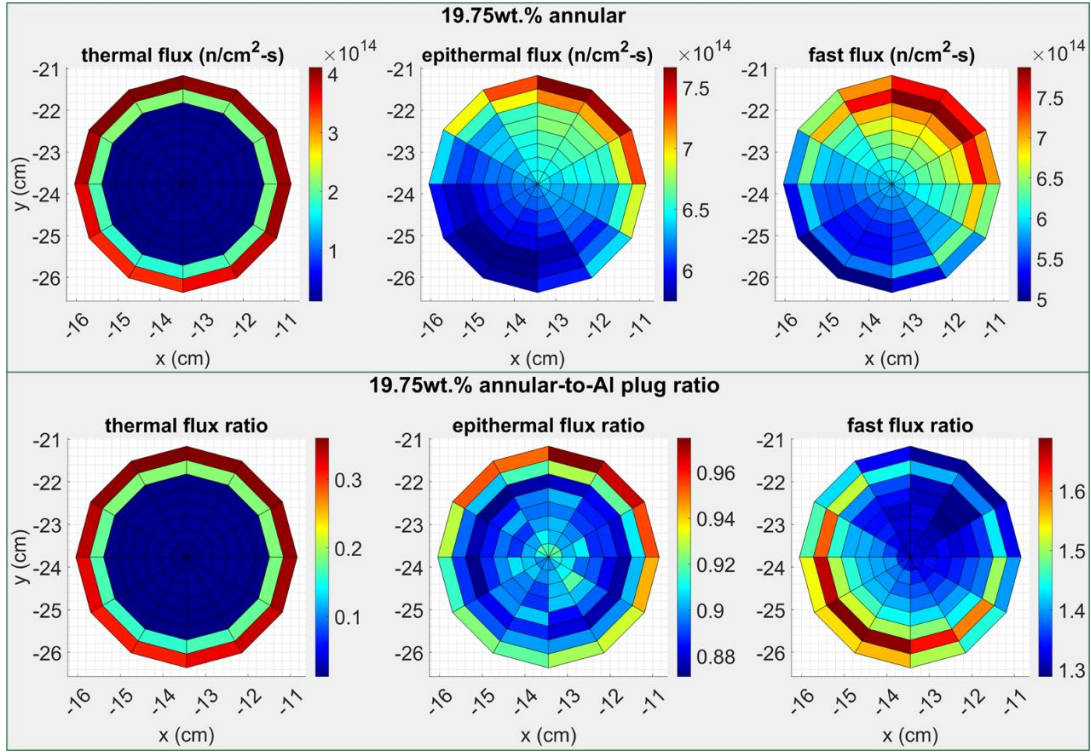
Figure 11. Three-energy group neutron flux distribution in the Gd poison filter plus fully annular 19.75 wt% U-10Mo fast-flux booster configuration and comparison to the reference Al plug case.
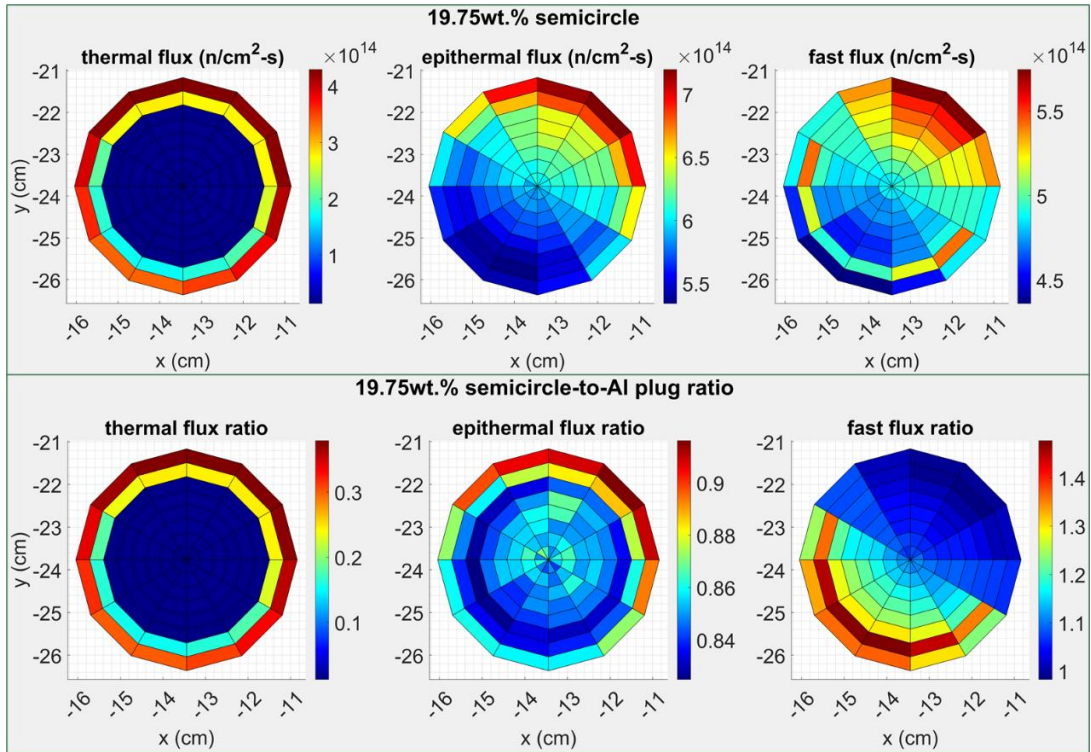
Figure 12. Three-energy group neutron flux distribution in the Gd poison filter plus semi-circle 19.75 wt% U-10Mo fast-flux booster configuration and comparison to the reference Al plug case.

4.1.3.2   PB reflector VXF calculations

The scoping calculations performed to evaluate the impact of fast-flux booster targets in the PB reflector VXFs focused on inner small VXF-14, outer large VXF-15, and inner small VXF-16. Emphasis was placed on large VXF-15 because the large facility offers a greater volume for experiments, especially when considering the volume occupied by the studied flux boosting targets. Three major differences between the RB and PB facilities are as follows (1) the fluxes are greater in the RB facilities, (2) the flux spectrum is harder in the RB facilities, and (3) changes in the PB have much less of an impact on core reactivity and physics.

As described briefly in Table 6, nine cases were developed for this study. Cases 1 and 9 are illustrated in Figure 13. The annular flux booster targets consisted of 50 mil (1.27 mm) thick plates and a central 15 mil (0.38 mm) thick LEU U-10Mo foil enriched to 19.75 wt% ^{235}U. Again, the simulated target was assumed to be an aluminum plug for the perturbed cases with flux boosters. Three-energy group flux distributions on the core midplane of the three VXFs were tallied on a superimposed six radial (0.40 cm Δr region for small VXFs, and 0.67 cm Δr region for large VXFs) by 12 azimuthal (30° Δθ regions) mesh.

Table 7 and Figure 14 summarize the impacts that the configuration perturbations have on reactivity and fast neutron fluxes. Small reactivity changes are calculated when replacing Be plugs with Al plugs or water-filled holes with stainless steel liners and orifices. Small-to-moderate reactivity increases are calculated for the cases in which booster targets are only placed in the large VXF-15; however, moderate-to-large increases are calculated for cases in which booster targets are also placed in the small VXFs.

Table 6. Description of PB reflector VXF configurations

Case	ISVXF-14	ISVXF-16	OLVXF-15
1	Be plug	Be plug	Be plug
2	Al plug	Al plug	Al plug
3	Water/SST liner	Water/SST liner	Water/SST liner
4	Be plug	Be plug	1 U-10Mo target
5	Be plug	Be plug	2 U-10Mo targets
6	Be plug	Be plug	3 U-10Mo targets
7	1 U-10Mo target	1 U-10Mo target	3 U-10Mo targets
8	2 U-10Mo targets	2 U-10Mo targets	3 U-10Mo targets
9	3 U-10Mo targets	3 U-10Mo targets	3 U-10Mo targets

ISVXF = inner small VXF
OLVXF = outer large VXF
SST = stainless steel
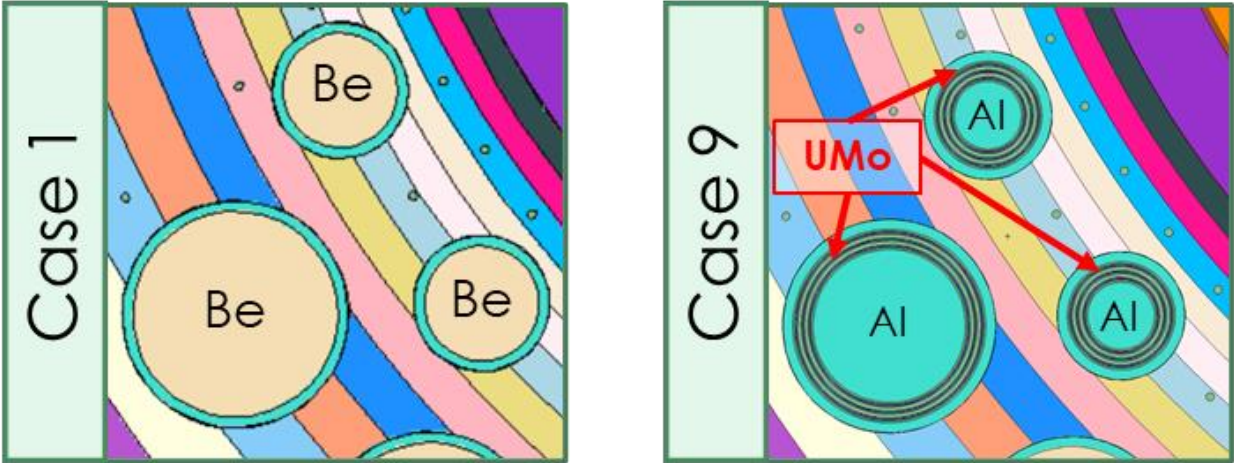
Figure 13. Midplane cross section of MCNP model cases 1 and 9.

Table 7. Summary of permanent reflector VXF fast neutron flux (n-cm^{-2}-s^{-1}) boosting results

Case	k$_{eff}$	Δk$_{eff}$ (¢)	ISVXF-14 fast flux			ISVXF-16 fast flux			OLVXF-15 fast flux		
			Min	Max[a]	CL[b]	Min	Max[a]	CL	Min	Max[a]	CL
1	1.00305	0.0	3.09E+13	6.54E+13	4.45E+13	3.20E+13	6.67E+13	4.58E+13	6.49E+12	2.39E+13	1.26E+13
2	1.00255	-6.8	3.79E+13	6.49E+13	5.01E+13	3.91E+13	6.58E+13	5.18E+13	1.15E+13	2.70E+13	1.80E+13
3	1.00243	-8.4	2.36E+13	5.48E+13	3.00E+13	2.36E+13	5.44E+13	3.03E+13	4.12E+12	1.63E+13	6.16E+12
4	1.00359	7.3	8.20E+13	1.24E+14	9.76E+13	8.47E+13	1.24E+14	1.00E+14	1.84E+14	2.78E+14	1.90E+14
5	1.00387	11.1	9.82E+13	1.61E+14	1.19E+14	1.01E+14	1.61E+14	1.21E+14	2.51E+14	3.77E+14	2.61E+14
6	1.00408	13.9	1.05E+14	1.79E+14	1.30E+14	1.09E+14	1.80E+14	1.33E+14	2.85E+14	4.50E+14	3.03E+14
7	1.00621	42.7	4.13E+14	5.68E+14	4.33E+14	4.37E+14	5.86E+14	4.46E+14	3.37E+14	5.15E+14	3.73E+14
8	1.00725	56.6	5.13E+14	7.39E+14	5.67E+14	5.40E+14	7.71E+14	5.85E+14	3.66E+14	5.52E+14	4.07E+14
9	1.00789	65.2	5.62E+14	8.19E+14	6.49E+14	5.88E+14	8.52E+14	6.74E+14	3.83E+14	5.78E+14	4.31E+14

a. Maximum values occur in the mesh cells containing U-10Mo fuel for the subject fast-flux booster cases
b. CL = centerline
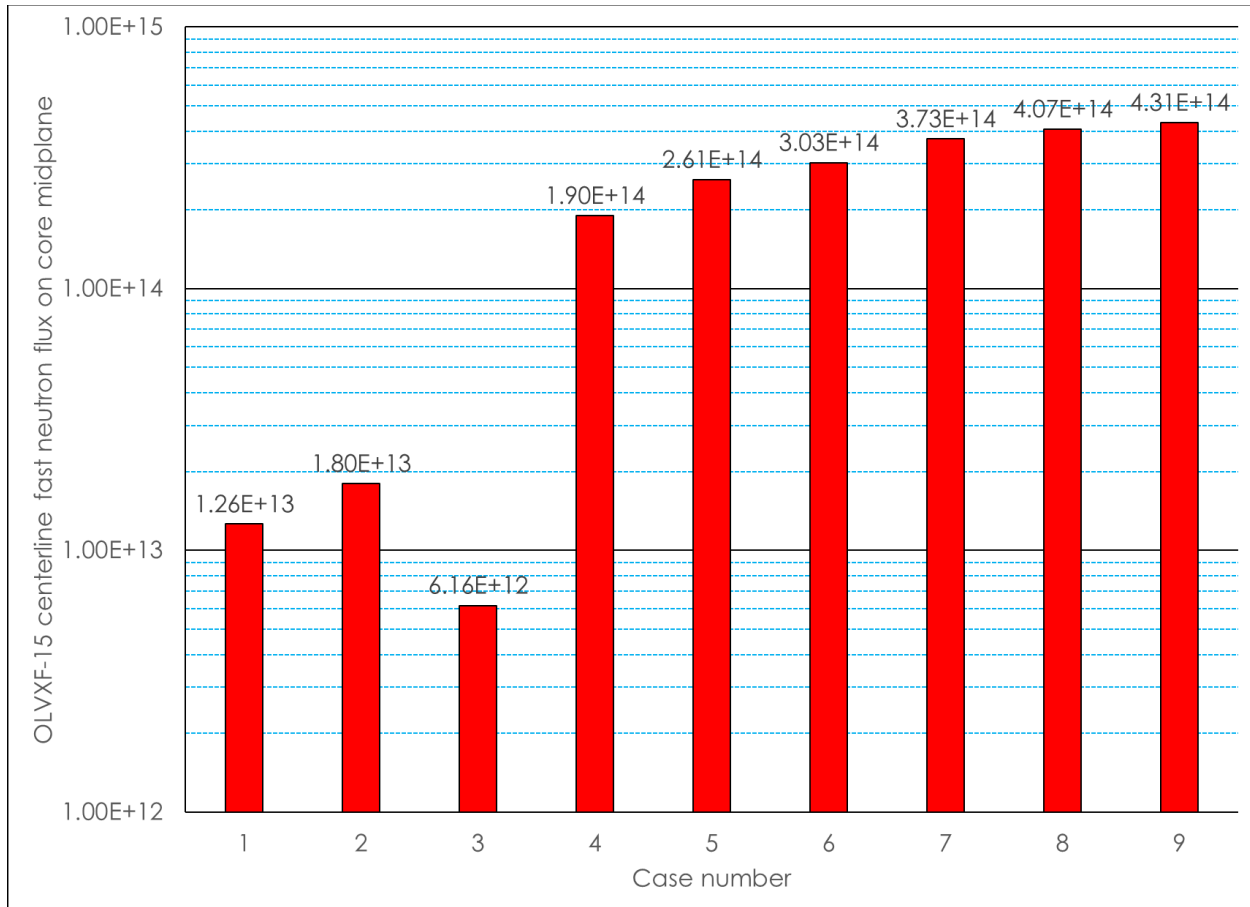
Figure 14. Flux-boosting target configurations' impact on outer large VXF-15 fast neutron flux.

4.1.4 Cost and Schedule Forecasting and Estimates

The costs associated with the various flux filter and booster concepts are expected to vary considerably, and they would depend on the use of fueled targets. For the fueled target concept designs, a qualified fuel form must be leveraged because qualifying a new fuel form for use in these targets would significantly increase the scope, schedule, costs, and risks.

Using the target design would require neutronics, thermal hydraulics, mechanical, experiment, and safety analysts to ensure that the design performs its intended function efficiently and safely. The costs associated with the target design would mostly consist of labor costs associated with the analysts' modeling, simulating, drawing, and evaluating the targets for use in the reactor. Additionally, a narrowed-down scope would likely be required to reduce the number of configurable options to pursue further. The calendar time required for this aspect of the work is estimated to be one to two years of effort, and the labor costs are estimated to be about $500k, ± $250k, depending on the number and type of designs being pursued. This rough estimate is based on experience with design and analysis tasks associated with other complex reactor components and irradiation experiments such as the RB-19J and discussions with staff involved in these activities.

Costs associated with fabrication, qualification, transportation, and handing of the subject targets are expected to make up the bulk of the total costs. These costs will vary drastically, depending on the design(s) being pursued. For example, a hafnium shield clad in aluminum would cost significantly less than multiple U-10Mo monolithic alloy foils clad in aluminum. Depending on the design and associated

26

requirements, these costs are estimated to be around $1–5M, and the time needed to perform these tasks range between approximately six months to two years. However, standardizing these targets would result in long-term cost and time savings. This rough estimate is based on experience with the fabrication of other complex irradiation experiments such as the RB-19J.

4.2   REFLECTOR CHANGES FOR ENHANCED IRRADIATION CONDITIONS

Preconceptual design ideas regarding reflector changes for enhanced irradiation conditions are described in this section. The general discussion in Section 4.1 regarding possible approaches to change the radiation environment and neutron spectrum holds true for this section. However, the preconceptual design ideas discussed in this section require changes to the beryllium reflector and are therefore considered integral to the reflector design.

A summary of the reflector change preconceptual design ideas is provided in Table 8. Options (1) and (2) involve modifying the size, location, and / or shape of beryllium reflector irradiation facilities. One or multiple large inner small VXF positions would enable larger experiments to be irradiated with higher fluxes than those obtainable in the large outer VXFs of the current reflector design. Additionally, a more rectangular design (or other geometric shape) may result in additional versatility and flexibility. This would allow for different experiment geometries / arrays and moderators / reflectors to be inserted into the experiment facility to tailor the radiation environment the experiment is exposed to. Option (3) involves machining small holes around the periphery of the beryllium reflector experiment facilities. The holes could be loaded with annular targets capable of boosting the fast flux (e.g., ^{235}U fueled targets), reducing the thermal flux (e.g., Eu, Gd, Hf), or producing radioisotopes (e.g., ^{238}Pu production targets). Lastly, Option (4) involves machining out an annulus around an experiment facility, where a non-moderating reflector (e.g., stainless steel) or other material could be located to alter the neutron flux energy distribution to the experiment.

4.2.1   Design Requirements

The design requirements discussed in Section 4.1.1 for the experiment facility flux boosters and filters concepts also apply to the beryllium reflector change concepts. Additional requirements are however required for the beryllium reflector change concepts because they represent a design modification to a core component and are therefore not simply considered an experiment. Therefore, introduction of the proposed changes should have no adverse effects on the beryllium reflector's ability to perform its intended function safely and reliably.
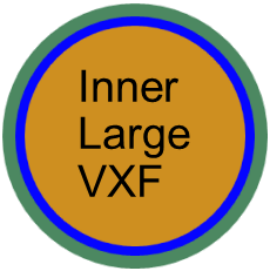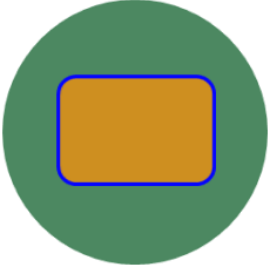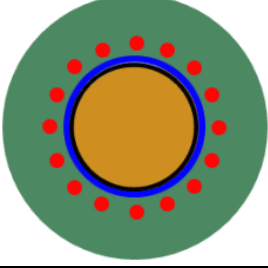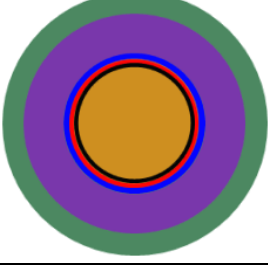
4.2.2   Limitations/Challenges

Manufacturing a large beryllium reflector is costly and time consuming, requiring several specialized companies to perform various manufacturing tasks (e.g., deep hole drilling). Furthermore, beryllium is a hazardous material, which limits the number of domestic companies that are willing to perform such operations. Therefore, priority should be taken to ensure that any changes made to the reflector would not notably increase the risks associated with fabrication.

4.2.3   Calculations

No supplemental calculations were performed in FY22 to support the beryllium reflector change concepts.

Table 8. Summary of reflector changes for enhanced irradiation preconceptual designs

Concept description	Concept illustration[*]
1. Redesign the PB reflector experiment layout to incorporate one or two inner large VXFs to accommodate larger experiment facilities in a higher flux region. Concurrent implementation of thermal and/or resonance filters and fast neutron flux boosters will provide additional spectrum tailoring benefits.	
2. Add a larger and/or a more modular experiment facility in the beryllium reflector to increase the versatility / flexibility for irradiations. Larger experiments of various geometries, surroundings (e.g., moderators, reflectors, filters, boosters) will be able to be irradiated.	
3. Add small annular experiment facilities around an experiment facility that could be loaded with fast neutron flux–boosting fuel rods or thermal and/or resonance filtering rods to provide additional capability to irradiate fuel and tailor the spectrum to the experiments' needs.	
4. Replace beryllium material surrounding a VXF with a non-moderating reflector material to increase fast flux to the experiment facility and to increase the efficiency of the internal fast neutron flux booster.	

⊙ beryllium reflector   ⊙ aluminum liner   ⊙ experiment   ⊙ neutron filter   ⊙ fast flux booster   ⊙ non-moderating reflector
(water coolant channels not depicted)

4.2.4   Cost and Schedule Forecasting and Estimates

The costs associated with the various beryllium reflector change concepts would not necessarily be significant. As part of the HFIR-CRITICAL efforts, potential reflector design and fabrication changes are being evaluated. Additionally, the cost and fabrication (e.g., billet, segmentation, testing, machining, and assembly) time of a new PB reflector is about $7–10M over 5–7 years, assuming that no changes are made to the currently qualified designs. The cost and timeline are based on conversations with domestic vendors and current experience in procuring a new PB reflector. Therefore, incorporating one or more of the spectrum tailoring–enabling preconceptual design changes into a future reflector would not significantly increase the scope of planned future tasks.

Reflector and experiment design activities would require neutronics, thermal hydraulics, mechanical, experiment, and safety analysts to ensure that the design performs its intended function efficiently and safely. The costs associated with the design and qualification aspects would mostly consist of labor costs associated with the analysts modeling, simulating, drawing, and evaluating the reflector for use in the reactor. The calendar time required for these tasks is estimated to be one to two years, which could be rolled into HFIR-CRITICAL efforts. The additional labor costs are estimated to be about $500k ± $250k. This rough estimate is based on recent PB reflector redesign efforts, mostly including reactor physics, thermal-hydraulics, structural, and safety analyses.

Costs associated with fabrication of the preconceptual design changes only, relative to a currently qualified reflector design, are expected to be on the order of $0–2M, depending on the design changes. In other words, this cost estimate is the assumed cost difference between fabrication of a currently qualified design and a design incorporating the proposed irradiation enhancement features. This cost difference is small-to-moderate when compared to the total cost to fabricate a new reflector. The additional cost estimate is based on engineering judgement and knowledge of costs associated with the fabrication of PB reflectors.

4.3 ION BEAM IRRADIATION FACILITY

When addressing the abundant challenges in developing structural alloys for next-generation nuclear power systems, it is critical that neutron exposure tests be conducted on any structural alloys being considered viable for reactor applications. Limitation in achievable high damage levels to evaluate the performance of candidate materials is, however, a bottleneck. Instead of physically tailoring neutron energy and flux an alternative approach is to *tailor recoil spectrum by energetic ions*, which provides desirable options and flexibilities for materials research, including reduced transmutations and higher dpa rates.

It is known that ion irradiation is the most amenable method to reach high doses in a reasonable time, so energetic ions are often used as a surrogate for neutrons. This approach has greatly accelerated the research and development (R&D) processes for investigating radiation effects in materials (Was 2007, Was 2014, IAEA 2018, Zinkle 2018). Ion irradiation is a highly accelerated approach, so its relevance to fission and fusion neutron irradiations must be addressed. Results from both ion and neutron irradiation facilities have been extrapolated to fission and fusion applications because irradiation parameters such as damage rates, gas production, and recoil spectra are similar or relevant to those of the corresponding nuclear energy systems (Guo 2016).

Unlike neutron irradiation, *ion irradiation has the advantages of well-controlled irradiation conditions (e.g., damage profiles, dose, dose rate, temperature) and easy sample handling (nonradioactive)*. For example, radiation-induced gas migration pathways (e.g., ^{4}He, ^{1}H or ^{2}H (D) migration and redistribution) and microstructure evolution in a nuclear material can be investigated under ion irradiation at fission/fusion relevant doses and temperatures. The candidate materials can be pre-implanted with He, H and D to desirable concentrations, and these pre-implanted samples can then be subjected to ion irradiations (e.g., He, Li, O, or other heavy ions) with varying energies (a few hundred keV to a few MeV) and dose rates (~10^{-1} to 10^{-4} dpa s^{-1}) at temperatures of ~ 800–1,000°C. Well-controlled ion irradiation studies allow separate effects to be analyzed to delineate various contributions to material degradation. Using different ion masses, energies, and fluxes, ion irradiation can cover a broad range of neutron recoil spectra and allow dose-rate studies, thus providing a path forward to emulate fission and fusion neutron regimes with confidence to develop strategies to enhance radiation tolerance (i.e., resist to degradation) and to predict material performance.

4.3.1 Design Requirements

The following discussion and examples address some important aspects of possible *recoil spectrum tailoring by ions*, demonstrating the need for radiation effects studies of nuclear materials. More specifically, the discussion establishes the means to bridge the gap between neutrons and ions for radiation effect studies. By tailoring recoil spectra and taking advantage of recent developments in (1) leadership computing capabilities, (2) advances in electronic structure codes, (3) physics-based simulation, and (4) deep learning techniques, complex transient defect processes can be addressed and taken into consideration to predict materials performance in various reactor environments.

4.3.1.1 Differences in irradiation parameters – ions vs. neutrons

Irradiation parameters from neutrons or ions mainly include *four fundamentally intertwined aspects*:
1. spatial distribution of defects,
2. recoil spectrum,
3. dose rates, and
4. temporal and spatial coupling of the thermal and athermal defect processes along the ion or recoil paths.

Furthermore, the effects of transmutation elements produced from neutron irradiation should not be overlooked. New scientific perspectives of exploiting ions to accelerate the damage evolution in a neutron-relevant manner require that the differences from the four aspects be understood and qualified.

Energetic charge particles interact with solids, inducing a *spatial distribution of defects* (Figure 15). Light charged particles such as electrons and protons may produce damage as isolated Frenkel pairs or in small clusters, whereas heavy ions and neutrons can create damage in large clusters (Was 1994, Was 2007, Averback 1994). At a given energy such as 1 MeV particle irradiation of Ni metal as shown in Figure 15, the cascade volume of neutrons is larger than that of electrons and ions.
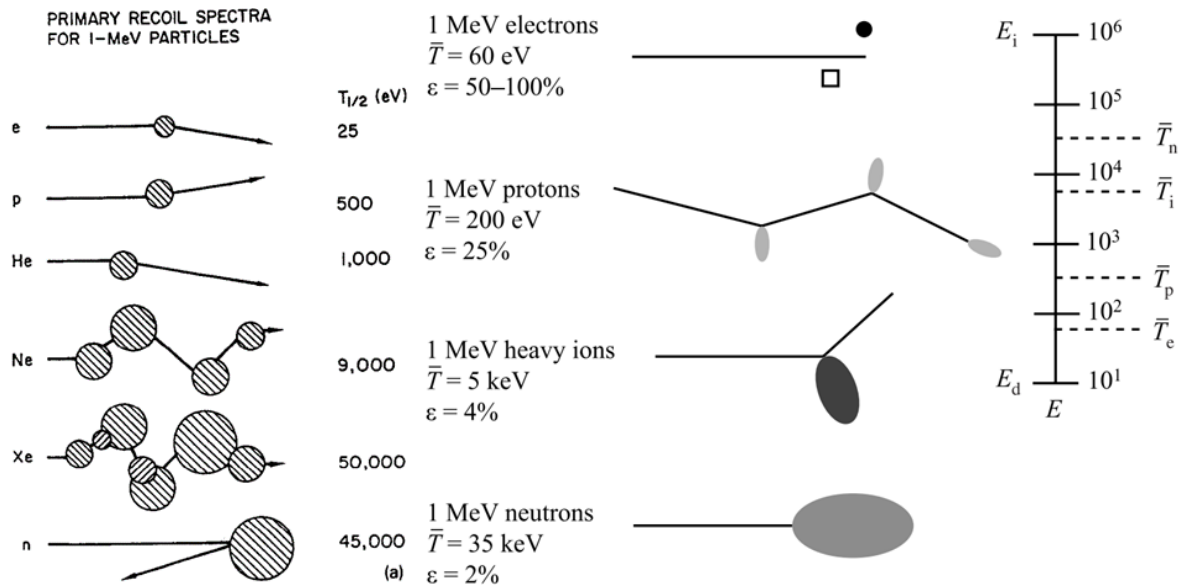
Figure 15. Difference in damage types produced by different particles. Difference in damage morphology, displacement efficiency, and average recoil energy for 1 MeV charged particles incident on Cu (left) (Averback 1994) and Ni (right) (Was 1994) metals.

Besides spatial distribution of defects, both *primary recoil spectrum* and *weighted recoil spectra* are important concepts. The density of recoils as a function of recoil energy is known as the *primary recoil spectrum*, which depends on the projectile energy and mass. *Primary recoil spectrum* (Figure 15) gives a measure of the density of displacement damage in the target. It is the probability distribution that describes the ability of a recoil atom to be ejected with a kinetic energy in the range [T, T + ΔT] for a defined k_{th} interaction. The Coulomb potential is a good approximation for proton irradiation, whereas the hard-sphere potential is a good approximation for neutron irradiation (Was 2007).

As stated in the textbook *Fundamentals of Radiation Materials Science* by Gary S. Was, the Coulomb forces extend to infinity and slowly increase as the particle approaches the target. In a hard-sphere interaction, the particles and target do not "feel" each other until their separation reaches the hard-sphere radius, at which point the repulsive force goes to infinity. A screened Coulomb is most appropriate for heavy ion irradiation. The result is that Coulomb interactions tend to create many primary knock-on atoms (PKAs) with low energy, whereas hard-sphere collisions create fewer PKAs, but with higher energy.

The primary recoil spectrum can be calculated from basic physical principles and measured neutron cross sections for all neutron–atom interactions. The primary recoil spectrum is thus able to define the averaged amount of energy transferred to recoils in a material by a given irradiation (Gabriel 1976, Lunéville

2006). To handle the total number of displaced atoms, a model of displacements per atom (dpa) must be introduced. The elementary interactions between projectiles and atoms must then be weighted by a defined number of displacements per atoms. A more realistic comparison of different kinds of irradiation can then be obtained from the calculation of the *weighted recoil spectrum* (i.e., the number of displacements produced by a recoil atom). In other words, the weighted average recoil spectrum is obtained by weighting the primary recoil spectrum against the number of defects or the damage energy produced in each recoil. The *weighted recoil spectrum* is thus also a key parameter to use when comparing the behavior of materials under irradiation.

As the most amenable method to reach high doses in a reasonable time frame, ion irradiation can produce tens to hundreds of dpa within a few hours. Because ion irradiation is an accelerated approach as a result of its much higher *dose rates* than those in reactor environments, the generally upward temperature shift of irradiation damage processes under high dose rate ion irradiation is generally used in predictive model development and the experiment design. This approach requires that ion irradiation studies be conducted over a much wider range of dose rates and higher temperatures than those that might be expected in a reactor environment. Understanding the effects of dose rates and irradiation temperatures on microstructural changes based on ion irradiation data can provide insights on the controlling defect kinetics that can be modeled to predict behavior at lower fission/fusion-relevant dose rates.

Furthermore, the noticeable differences in temporal and spatial scales of ion and fission/fusion neutron irradiations present unique challenges. Because of the large amount of energy transfer to target electrons, energetic charged particles irradiation induces far from equilibrium athermal processes: that is, inelastic thermal spikes or athermal defect processes. It also induces radiation-enhanced diffusional process such as modified energy barriers caused by charge-redistribution that differ from thermal equilibrium conditions such as annealing at high temperatures. Although neutrons do not lose energy to target electrons, fusion neutrons do produce energetic recoils, and some are at MeV energies. For example, PKAs from fusion neutrons (or spallation neutrons used to simulate fusion neutrons) can be several MeV, so they are similar to ion irradiation. Both energetic ions and recoils induce defect processes that are consequences of *the spatial and temporal coupling of atomic displacement events and energy dissipation from ionization*. In candidate ceramic materials, ionization can rupture or change the nature of ionic bonds and modify valence electron distributions, which in turn can result in the formation of charged defects, enhanced defect, and atomic mobilities (Itoh 2001, Zhang 2014). Moreover, electronic energy losses lead to highly localized inelastic thermal spikes (<100 ps) that can result in phase transformations or instability. Athermal effects can cause defect recovery, strain relaxation, gas and defect diffusion, phase transformations, and gas resolution from bubbles. Such transient irradiation-induced processes are experimentally well documented in the literature for ceramics (Lang 1976, Lomako 1980, Lang 1982, Assmann 1978, Matzke 1983, Matzke 2000, Zinkle 2002) under neutron, fission, ion, electron and laser irradiations. These processes are often referred to as *athermal* because they are temperature independent or weakly dependent on temperature and cannot be described as thermally activated (activation energies below 0.2 eV). However, they are generally proportional to the neutron/ion flux or fission rate. In ion irradiation studies as surrogate for neutrons, the athermal effect from ions, which is different from relatively low electronic excitation of reaction products or along the PKA trajectories, can be quantified by changing ion mass and energies and should be taken into consideration for material performance assignments.

4.3.1.2 Ion beam facility

Diminishing research and training capabilities in the United States for ion beam analysis (IBA) and ion beam modification, as well as fundamental understanding of ion–solid interaction and radiation effects research in materials prompted the University of Tennessee (UT) to partner ORNL to develop a multifunctional Ion Beam Materials Laboratory (IBML, http://ibml.utk.edu/) in 2010. IBML is located on

the UT campus (Zhang 2014) and was designed to address the scientific challenges associated with fundamental and applied programs, as well as educational and training needs (Zhang 2014). An onsite ion beam facility with terminal voltage similar to IBML accelerator (i.e., 3 MV), 5 MV, or much higher, thus enabling intermediate energy proton irradiation with energy ranging from 10–30 MeV (Jepeal 2021) at or near HFIR, will enhance fundamental research on ion–solid interaction, ion beam analysis, ion beam modification, reactor-based nuclear material research, and other basic and applied research on irradiation effects in a wide range of materials.

The possible high throughput assessment of materials under reactor-relevant conditions enabled by MeV ion accelerators and intermediate energy proton irradiation will accelerate the pace of engineering-scale radiation damage testing and will allow for quicker, more effective design of nuclear energy systems as follows:
- Higher dpa rates, together with no or reduced transmutations, that are desirable for materials research
- Tailored recoil spectrum as tools for fast and efficient creation of radiation damage; examples of *recoil spectrum tailoring by ions* provided below for details
- Ion beam analysis techniques for materials property characterization, including identification and monitoring a broad range of isotopes and elements (Hauck 2023)

An onsite ion facility would enable rapid materials development using ion irradiation, including:
1. Self-ion irradiation (e.g., H, He, O, Si and Ti) can be conducted at required energy, dose rate and temperatures to evaluate **thermally** *induced* and **radiation**-*induced* gas migration and their impact on microstructure.
2. Heavy ions produce high-energy recoils, deposit significant amounts of energy within a small volume, create **dense cascades** and thus **high dose rates**, and consequentially extended defects and large defect clusters.
3. Light ion or proton irradiation, in which knock-on collision is similar to that of neutrons, is often used to investigate scattered knock-on damage from neutrons. Simple defects and scattered small clusters are expected.

This type of facility could also be used for IBA (e.g., on-line or in-situ, real time) to provide onsite analysis tools such as:
1. Understanding ^{1}H, ^{2}H (D), and ^{4}He migration, interactions, and redistribution in candidate materials under ion irradiation at fusion-relevant doses and temperatures.
2. Pre-implanting candidate materials with He, H, and/or D to desired concentrations. Pre-implanted samples can then be subjected to thermal treatment and additional ion irradiation to study (a) thermal migration and trapping/detrapping at defects created during implantation, (b) irradiation-enhanced gas/defect dynamics, (c) the effects of He on the migration and trapping of H isotopes, and (d) synergies of He and H on microstructure evolution, such as promotion of He bubble formation by H.
3. Examining radiation-induced trapping and migration of elemental gases, microstructure changes, and mechanical behavior using a suite of complementary microstructural characterization tools, and by online IBA techniques, including Rutherford backscattering spectrometry (RBS), nuclear reaction analysis (NRA), and time-of-flight elastic recoil detection analysis (ToF-ERDA).
4. Using the high sensitivity of IBA techniques to determine gas element concentrations and changes in cation/oxygen content. Moreover, release of H isotopes under ion irradiation can be measured directly using ToF-ERDA.
5. Investigating the irradiation-induced release of H isotopes as a function of temperature under the range of operating temperatures and temperature gradients expected in reactor environments. The results will inform the design and modeling of T recovery and inventory, as well as fuel cycles analysis.

The inclusion of tube connections to the core would enable enhanced research opportunities.

4.3.2   Calculations and Examples

Supplemental calculations and examples demonstrating the benefits of ion beam facilities are provided in Appendix B.

4.3.3   Cost and Schedule Forecasting and Estimates

It is envisioned that two to three ion sources would be deployed at HFIR. Either 5 or 6 MV Tandem accelerators, together with a few target endstations and some ion beam analysis techniques/systems, are estimated to cost about $5–6M. The target end stations must be capable of handling radioactive and nonradioactive samples or reactions. An ion lab with a 3 MV Tandem accelerators (cost ~ $3.5M) is illustrated in Figure 16 (Zhang 2014). The total cost to design and deploy the HFIR ion beam facility is estimated to be on the order of $20–100M and is estimated to take 2–5 years to complete. The cost and timeline estimates are based on extrapolating those associated with the IBML on the UT campus to the beam facility envisioned at HFIR.
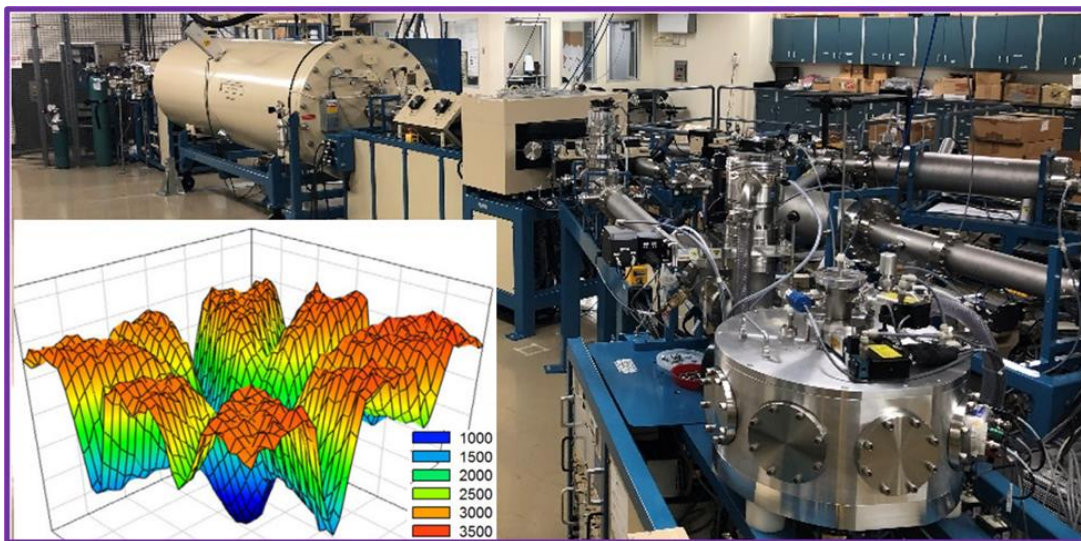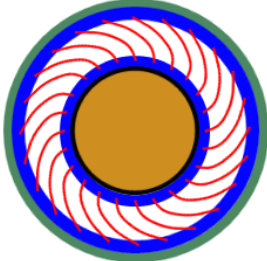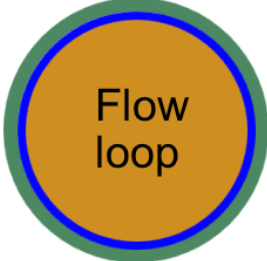

Figure 16. Illustration of the ion beam facility on the UT Knoxville campus (Zhang 2014).

4.4 OTHER OPTIONS DISCUSSED

Table 9 summarizes three additional preconceptual design ideas that were discussed but not pursued in detail by the Spectrum Tailoring Working Group. Option 1 involves the design and deployment of a miniature reactor in the PB reflector or in the reactor pool, radially outboard of the beryllium reflector and cage. This option would result in another high-flux FTT, but it would also require significant increases in fuel, modifications to the reactor, and changes to the safety basis. Option 2 considers a flow loop that could enable controlled flow of moderators or poisons for additional spectrum tailoring capabilities, but this option was not explored because a separate working group is evaluating flow loops. Lastly, Option 3 involves major changes to the reactor's reactivity and safety control systems, which would result in major design and safety basis changes. Each of these options could enhance the in-core irradiation science performed at HFIR and may be considered later.

Table 9. Summary of preconceptual design ideas discussed but not considered in detail

Concept description	Concept illustration
(1) Deployment of a miniature HFIR in the PB reflector or in the reactor pool. A single fuel element surrounding a flux trap will provide an additional flux trap for in-core irradiation purposes. The flux trap could be used for (a) large experiment irradiations like in RB* and VXF irradiations or (b) capsule irradiations in target rods like in the central flux trap.	Be reflector · Involute fuel plates · Al side plates · Experiment · Optional poison filter
(2) A flow loop facility integrated with a beryllium reflector irradiation facility could be used to control a flowing liquid around or through an experiment. For example, borated water could be used to reduce the thermal neutron flux, or a liquid fuel could be used as a fast neutron flux booster.	Be reflector · Al liner · Experiment and flowing liquid
(3) Major changes to the control system, such as moving the control elements between the fuel elements or into the flux trap region (e.g., like FRM-II or RHF), may increase the neutron flux to the beryllium reflector experiment facilities and could produce a more axially flat and consistent flux profile during the cycle. A flowing liquid such as borated water could be considered in the control element region.	Be reflector · Fuel elements · Flux trap · Control elements

5. SPECTRUM TAILORING BENEFITS

One of HFIR's primary missions is to support research focused on neutron irradiation effects on materials properties. The preconceptual design options presented in this report are the authors' perspectives on how to best prepare HFIR to support the ever-changing needs of research programs and proof-of-concept testing at higher technology readiness levels (TRLs) to determine neutron irradiation effects on materials properties. Thermal conductivity and strength/ductility are two examples of properties that can affect heat transfer within the reactor or component reliability. As mentioned in Section 2.2, neutron spectrum tailoring, as well as possible recoil spectrum tailoring by ions described in in Section 4.3, must be explored to advance fundamental knowledge about the effects of radiation on materials and to support materials development and qualification efforts for the design, construction, and operation of the next generation of advanced nuclear fission and fusion reactors.

Near-term needs include development of methods to support materials studies for fast neutron spectrum fission reactor designs (e.g., TerraPower's three fast reactor concepts: Traveling Wave Reactor, Molten Chloride Fast Reactor, and the Natrium Sodium Fast Reactor, as well as other Gen-IV concepts such as lead-cooled fast reactors and other molten salt fast reactor designs), and materials for fusion reactors. The neutron energy spectrums of these reactors are significantly different than those of HFIR, but the use of different experimental configurations (e.g., removal of moderating material between the fuel and the materials being studied, the addition of thermal neutron shields around the experiments, or the addition of flux boosting fuel within or around the irradiation capsules) could assist with tailoring the neutron flux spectrum to be more prototypic to user needs.

A primary concern for advanced reactor designers is the amount of time necessary to obtain information about the effect of neutron irradiation on materials at the damage levels approaching reactor lifetime neutron fluences. Even with the extremely high fast neutron flux available in the HFIR FTT, most materials require 5–6 HFIR cycles to accumulate the same neutron fluence that the material will experience in ~10 years of power reactor operation. Therefore, if designers require data on materials with a planned 40-year in-reactor lifetime, those same materials require ~20 HFIR cycles, equating to roughly 4 years of irradiation in the HFIR FTT (assuming 5 cycles per year). This leads to the proposed spectral tailoring that would allow for an overall increase of the fast neutron flux for a specific experiment. These options would dramatically reduce the total irradiation time needed for materials development/qualification for advanced fission reactors.

More generalized spectrum tailoring over a broader energy range could benefit future reactor designs, but more importantly, it could become a revolutionary process to enable fundamental materials irradiation studies. These concepts could include a combination of thermal or resonance boosters for use in design irradiation experiments with a limited neutron energy range, providing insights into the difference in materials response to targeted neutron energies.

Another form of spectrum tailoring relevant to materials properties is to flatten the flux profile across the radial distance of the larger irradiation facilities in the HFIR reflector (RB, inner small [VXF] ISVXF, outer small VXF [OSVXF], and large VXF [LVXF] positions). These irradiation facilities are necessary for materials irradiations as composite materials are explored for advanced reactor uses. No data are available about how modifications to the composite component's physical attributes (e.g., reducing diameter of a tube to fit into a flux trap capsule) will affect changes to the component's properties as it is exposed to irradiation. As such, it is expected that larger irradiation facilities will be necessary to support these studies. The factor-of-two difference in flux between the inner and outer radial distances of these reflector irradiation positions introduce additional concerns, the primary concern being that the flux differences across these components could easily result in internal stresses caused by localized differences

in changing dimension, elastic properties, or thermal properties. Buildup of internal stresses could cause component failure, or at a minimum, these stresses could perturb the change of the materials properties or make the changes nonuniform throughout the component.

The final flux or recoil spectrum tailoring option (see Section 4.3) is the addition of an onsite ion irradiation facility (Hauck 2023) that will provide stand-alone and coordinating capabilities that can increase and enhance current HFIR missions. ORNL has led the use of accelerators and ion beams to study irradiation effects in materials. In the 1950s, the first 5.5 MV CN-Van de Graaff accelerator was used for nuclear physics research, and in the late 1960s and early 1970s, the mission of the accelerator was refocused to perform heavy ion irradiation damage studies (Lewis 1975). In the mid- to late-1970s, the setup was modified with the addition of a 400 kV Van de Graaff accelerator to allow for some of the first dual-beam irradiations (Packan 1980, Lewis 1979), in which injection of He^+ and H^+ ions was performed in conjunction with heavy ion irradiations to study the combined effect of gas production with radiation damage. During this same time, an in-situ irradiation creep setup was developed for the Oak Ridge Isochronous Cyclotron (ORIC) (Reiley, Auble, and Shannon 1980; Reiley, Auble, Beckers et al. 1980). The final modification to the accelerator program was the development of the triple ion beam chamber in the mid-1980s (Lewis 1988, Lewis 1989) that could perform simultaneous injection of He^+ and H^+ ions while producing irradiation damage via heavy ion irradiations. This final configuration also included an in-situ creep chamber, making the ORIC obsolete. Research performed in this triple beam facility was instrumental in supporting development of the targets for the ORNL Spallation Neutron Source (Lee 1999). The ion beam facility at ORNL was shut down and decommissioned in the late 1990s, and no new relevant capability has been installed at ORNL. Redevelopment of these capabilities will allow for more tailored research into materials for advanced fission and fusion reactors. Performing irradiation damage studies in materials with an ion beam facility would be one of the primary missions of a new ion beam facility. Additionally, this could provide a research pathway that has been minimally utilized in which the new ion beam would be used to pre-implant gasses of specific species into materials prior to irradiation in HFIR. This would better emulate the gas evolution in a fusion reactor environment, a factor not currently produced in HFIR because the high-energy neutrons (~14 MeV) needed for this gas production are absent from HFIR's neutron spectrum.

The ability to tailor the neutron spectrum within the HFIR FTT and reflector irradiation positions will open new avenues for irradiation programs that were previously unobtainable, such as research on the fundamentals of irradiation damage in materials for specified neutron energies, the use of thermal neutron shields/absorbers to obtain more applicable neutron energy spectra for fast fission and fusion reactor materials studies, and flattening the HFIR reflector's fast neutron flux profile to increase the usability of the reflector's irradiation positions for studies in composite materials. The addition of an ion beam facility will be coordinated with HFIR enhancements to provide additional, complementary means for producing irradiation damage and ion beam–based in-situ or off-line characterization methods not currently available at ORNL. This will facilitate new fundamental science programs on mechanical behavior and radiation effects (DOE-Basic Energy Sciences), programs supporting current reactor lifetime extensions and advanced fission reactor development (DOE-Nuclear Energy), and programs supporting the work necessary to successfully build and operate a fusion reactor (DOE-Fusion Energy Sciences). These topics are not only of interest within the United States: interest is also global for all future nuclear energy production means.

6. CONCLUSIONS

In response to the 2020 US DOE BESAC review, the HFIR-SENSe Initiative was established to provide a preconceptual assessment of hardware, systems, and infrastructure. The efforts associated with this initiative are being pursued to ensure that HFIR operates safely, reliably, and at an exceptionally high-performance level well into the future to support domestic and international neutron science–based research. In-core irradiation experiment research, such as materials and fuels irradiation research, is a primary mission of ORNL and HFIR. In support of HFIR-SENSe, a technically diverse group of ORNL irradiation research subject matter experts formed the Spectrum Tailoring Working Group with the goal of developing a compendium of experiment facility concepts capable of enhancing irradiation experiment conditions via neutron spectrum tailoring. This report documents the efforts performed in FY22, and pending the future direction of HFIR-SENSe and interest from other sponsors, these efforts may be continued in FY23 and beyond.

ORNL has been a leading institution in the field of radiation materials science since Eugene Wigner first discussed the possibility of neutrons and gamma rays affecting materials properties. The primary focus of radiation materials science is to understand and quantify how the interaction of radiation with solids changes materials properties, and how these changes affect the usable lifetime of these materials. The irradiation of materials in HFIR supports programs for DOE, international collaboration, and private industry. Reactor and experiment design enhancements capable of tailoring the neutron energy spectrum have the potential to significantly improve ORNL's materials irradiation research capabilities. The Spectrum Tailoring Working Group discussed and evaluated many ideas to improve spectrum tailoring capabilities in HFIR's beryllium reflector experiment facilities. Four primary objectives of a spectrum tailoring experiment facility were identified:
1. ability to significantly reduce the thermal neutron flux to the experiment
2. ability to increase the fast neutron flux to the experiment for increased displacements per atom
3. ability to modify the full neutron energy spectrum to better mimic user-desired conditions
4. ability to flatten the neutron flux profile across the experiment

An example of the need to control the neutron energy spectrum relates to the study of tungsten as a divertor material for tokamak fusion reactors. Exposure of tungsten to a high thermal neutron flux is not typical of a fusion environment and results in an undesirably high transmutation rate. Other needs related to controlling the neutron energy spectrum originate from both fission and fusion reactor applications. Materials irradiation research to support fission and fusion reactor applications would be significantly enhanced by the capability to increase the fast neutron flux and to tailor the energy spectrum to better mimic prototypic radiation environments. Spectrum tailoring could also provide a spatially uniform neutron flux across a material being irradiated for materials qualification testing. Large flux gradients across materials such as CMCs result in nonuniform dimensional changes that could lead to the buildup of internal stresses, fundamentally altering the material property changes caused by irradiation.

The spectrum tailoring preconceptual design ideas were binned into three categories: (1) internal experiment facility flux boosters and filters, (2) reflector changes for enhanced irradiation conditions, and (3) an ion beam facility. Fast neutron flux boosters containing fissile material (e.g., ^{235}U) near experiments can be used to produce fast neutrons via fission, exposing the experiments to a harder neutron flux spectrum. Conversely, neutron filters can be used to significantly reduce neutrons in certain energy ranges. For example, the use of a Gd filter surrounding an experiment would result in a significant reduction to the thermal neutron flux. These types of features could either be fabricated as experiments located within an experiment facility (e.g., RB, VXF) or into the beryllium reflector design. The use of boosters, filters, or a combination of the two has the potential to accomplish the four primary objectives.

Furthermore, the addition of an onsite ion beam irradiation facility would provide stand-alone and coordinating capabilities that would advance HFIR's missions. This capability would allow for more tailored research into materials for advanced fission and fusion reactors. Performing irradiation damage studies in materials with an ion beam facility would be one of the primary missions of a new ion beam facility. Additionally, the new ion beam could be used to pre-implant gasses of specific species into materials prior to irradiation in HFIR, which would better emulate gas evolution such as that which would occur in a fusion reactor environment.

Enhancing the ability to tailor the neutron flux spectrum within HFIR experiment irradiation positions and deploying an onsite ion irradiation facility would open new avenues for irradiation programs that were previously unobtainable. The new capabilities would serve domestic and international interests in support of current and future fission- and fusion-based nuclear energy production systems.

7. ACKNOWLEDGMENTS

8. REFERENCES

ASME (American Society of Mechanical Engineers). 2021. "2021 ASME Boiler and Pressure Vessel Code, Section III Rules for Construction of Nuclear Facility Components, Division 5 High Temperature Reactors," New York, The American Society of Mechanical Engineers.

Assmann, H. and H. Stehle. 1978. "Thermal and In-Reactor Densification of UO_2: Mechanisms and Experimental Results," *Nucl. Eng. Design* 48, 49–67.

Averback, R.S. 1994. "Atomic Displacement Processes in Irradiated Metals," *J. Nucl. Mater.* 216 49–62.

Report of the Basic Energy Sciences Advisory Committee (BESAC). 2020. "The Scientific Justification for a US Domestic High-Performance Reactor-Based Research Facility," US Department of Energy Office of Science. doi: https://doi.org/10.2172/1647598.

Bryan, C.D. and D. Chandler. 2023. *HFIR Futures - Enhanced Capabilities Series: Volume 1: Introduction to the HFIR Futures – Enhanced Capabilities Series*, ORNL/TM-2022/2691/V1, Oak Ridge National Laboratory.

Chadwick, M.B., et al. 2006. "ENDF/B-VII.0: Next Generation Evaluated Nuclear Data Library for Nuclear Science and Technology," *Nuclear Data Sheets* **107**, 2931–3060.

Chandler, D., C.D. Bryan, and J.L. McDuffee. 2022. "Enhancement Concept Reactor Physics Studies to Support HFIR Upgrade Planning Activities," *Proceedings of the International Conference on Physics of Reactors (PHYSOR 2022)*, Pittsburgh, PA, USA.

Chandler, D. and J. Navarro. 2022. *Reactor Physics Simulations of the High Flux Isotope Reactor Permanent Beryllium Reflector Number 5*, ORNL/TM-2022/2428, Oak Ridge National Laboratory. doi: https://doi.org/10.2172/1876305.

Chandler, D. and C.D. Bryan. 2021. "High Flux Isotope Reactor (HFIR)," In: E. Greenspan, (Ed.), *Encyclopedia of Nuclear Energy* 4. Elsevier, 64–73. doi: https://doi.org/10.1016/B978-0-12-819725-7.00051-9.

Chandler, D., B.R. Betzler, E.E. Davidson, and G. Ilas. 2020. "Modeling and Simulation of a High Flux Isotope Reactor Representative Core Model for Updated Performance and Safety Basis Assessments," *Nuclear Engineering and Design*, 366, 110752. doi: doi.org/10.1016/j.nucengdes.2020.110752.

Daily, C. 2016. *Heat Generation Rates in Gadolinium-Shielded Experiment RB19J in Position RB-5B of the HFIR Beryllium Reflector*, C-HFIR-2016-010 Rev. 1. Internal archived document that may be made available upon request to the Research Reactors Division Director.

Gabriel, T.A., J.D. Amburgey, N. M. Greene. 1976. *Radiation-Damage Calculations: Primary Recoil Spectra Displacement Rates, and Gas-Production Rates*, ORNL/TM-516Q.

Garrison, L.M., Y. Katoh, J.W. Geringer, M. Akiyoshi, X. Chen, M. Fukuda, A. Hasegawa, T. Hinoki, X. Hu, T. Koyanagi, E. Lang, M. McAlister, J. McDuffee, T. Miyazawa, C. Parish, E. Proehl, N. Reid, J. Robertson, and H. Wang. 2019. "PHENIX US-Japan Collaboration Investigation of Thermal and Mechanical Properties of Thermal Neutron–Shielded Irradiated Tungsten," *Fusion Science and Technology* 75, 499–509.

Griffiths, M. and R. Boothby. 2020. "3.09 - Radiation Effects in Nickel-Based Alloys," in *Comprehensive Nuclear Materials* (Second Edition), R.J.M. Konings and R.E. Stoller, Eds, Elsevier, Oxford, 334–371.

Guo, D. C. He, H. Zang, P. Zhang, L. Ma, T. Li, and X. Cao. 2016. "Re-Evaluation of Neutron Displacement Cross Sections for Silicon Carbide by a Monte Carlo Approach," *J. Nucl. Sci. Technol.* 53:2, 161–172.

Guo, D. H. Zang, P. Zhang, J. Xi, T. Li, L. Ma, and C. He. 2014. "Analysis of Primary Damage in Silicon Carbide under Fusion and Fission Neutron Spectra," *J. Nucl. Mater.* 455, 229–233.

Hashimoto, N., R. Kasada, B. Raj, and M. Vijayalakshmi. 2020. "3.05 - Radiation Effects in Ferritic Steels and Advanced Ferritic-Martensitic Steels," in *Comprehensive Nuclear Materials* (Second Ed.), R.J.M. Konings and R.E. Stoller, Eds., Elsevier, Oxford, 226–254.

Hauck, G., D. Bowen, D. Chandler, Z. Karriem, J. Powers, and Y. Zhang. 2023. *HFIR Futures - Enhanced Capabilities Series: Volume 9: Critical Facility with Add-On Ion Beam*, ORNL/TM-2022/2691/V9, Oak Ridge National Laboratory.

IAEA (International Atomic Energy Agency). 2018. Accelerator Simulation and Theoretical Modelling of Radiation Effects in Structural Materials, IAEA Nuclear Energy Series Publications, No. NF-T-2.2, Structure of The IAEA Nuclear Energy Series. ISSN 1995–7807, IAEAL 18-01158 | ISBN 978–92–0–107415–7.

Itoh, N. and A. M. Stoneham. 2001. *Materials Modification by Electronic Excitations*, Cambridge Univ. Press, Cambridge, United Kingdom.

Jepeal, S.J. L. Snead, and Z.S. Hartwig. 2021. "Intermediate Energy Proton Irradiation: Rapid, High-Fidelity Materials Testing for Fusion And Fission Energy Systems," *Mater. Des.* 200 109445.

Katoh, Y., L.L. Snead, L.M. Garrison, X. Hu, T. Koyanagi, C.M. Parish, P.D. Edmondson, M. Fukuda, T. Hwang, T. Tanaka, and A. Hasegawa. 2019. "Response of Unalloyed Tungsten to Mixed Spectrum Neutrons," *J. Nucl. Mater.* 520, 193–207.

Katoh, Y., L.L. Snead, C.M. Parish, T. Hinoki. 2013. Observation and possible mechanism of irradiation induced creep in ceramics. *J. Nucl. Mater.* 434, 141–151.

Lang, D.V. 1982. "Recombination-Enhanced Reactions in Semiconductors," *Ann. Rev. Mater. Sci.* 12, 377–400.

Lang, D.V. and L.C. Kimerling. 1976. "Observation of Athermal Defect Annealing in GaP," *Appl. Phys. Lett.* 28, 248–250.

Lee, E.H., J.D. Hunn, G.R. Rao, R.L. Klueh, and L.K. Mansur. 1999. "Triple Ion Beam Studies of Radiation Damage in 9Cr–2WVTa Ferritic/Martensitic Steel for a High Power Spallation Neutron Source," *J. Nucl. Mater.* 271-272, 385–390.

Lewis, M.B, F.K. McGowan, C.H. Johnson, M.J. Saltmarsh, and D. Kramer. 1975. "Oak Ridge CN Van de Graaff Facility for Heavy Ion Radiation Damage Studies," Presented at *Symposium on Experimental Methods for Charged-Particle Irradiations*, Gatlinburg, Tennessee, 30 Sep.

Lewis, M.B., N.H. Packan, G.F. Wells, and R.A. Buhl. 1979. "Improved Techniques for Heavy-Ion Simulation of Neutron Radiation Damage," *Nucl. Instrum. Methods* 167, 233–247.

Lewis, M.B., W.R. Allen, R.A. Buhl, N.H. Packan, S.W. Cook, and L.K. Mansur. 1988. *Triple Ion Beam Irradiation Facility*, ORNL/TM-10867, Oak Ridge National Laboratory.

Lewis, M.B., W.R. Allen, R.A. Buhl, N.H. Packan, S.W. Cook, and L.K. Mansur. 1989. "Triple Ion Beam Irradiation Facility," *Nucl. Instrum. Methods Phys. Res. B*, 43, 243–253.

Lomako, V.M., and A.M. Novoselov. 1980. "Athermal Annealing of Structure Damage in GaAs," *Phys. Stat. Sol. A* 60, 557–564.

Lunéville, L., D. Simeone, and C. Jouanne. 2006. "Calculation of Radiation Damage Induced by Neutrons in Compound Materials," *J. Nucl. Mater.* 353, 89–100.

Matzke, H.J. P.G. Lucuta, and T. Wiss. 2000. "Swift Heavy Ion and Fission Damage Effects in UO_2," *Nucl. Instrum. Methods Phys. Res. B*, 920, 166–167.

Matzke, H.J. 1983. "Radiation Enhanced Diffusion in UO_2 and $(U,Pu)O_2$," *Radiat. Eff.* 75, 317–325.

Nuckols, L., M. L. Crespillo, Y. Yang, J. Li, E. Zarkadoula, Y. Zhang, and W. J. Weber. 2021. Effects of Recoil Spectra and Electronic Energy Dissipation on Defect Survival in 3C-SiC," *Materialia* 15, 101023.

Ostrouchov, C., Y. Zhang, and W.J. Weber. 2018. "pysrim: Automation, Analysis, and Plotting of SRIM Calculations," *J. Open Source Softw.* 3, 10–12.

Packan, N.H., and R.A. Buhl. 1980. *Multispecimen Dual-Beam Irradiation Damage Chamber*, ORNL/TM-7276, Oak Ridge National Laboratory, Oak Ridge, TN.

Pickering, E.J., A.W. Carruther, P.J. Barron, S.C. Middleburgh, D.E.J. Armstrong, and A.S. Gandy. 2021. "High-Entropy Alloys for Advanced Nuclear Applications." *Entropy* 23, 1–28. https://doi.org/10.3390/e23010098.

Reiley, T.C., R.L. Auble, and R.H. Shannon. 1980 "Irradiation Creep under 60 MEV Alpha Irradiation," *J. Nucl. Mater.* 90, 271–281.

Reiley, T.C., R.L. Auble, R.M. Beckers, E.E. Bloom, M.G. Duncan, M.J. Saltmarsh, and R.H. Shannon. 1980. *ORNL Irradiation Creep Facility*, ORNL/TM-7470, Oak Ridge National Laboratory, Oak Ridge, TN.

San, S., Y. Tong, H. Bei, B. Kombaiah, Y. Zhang, and W.-Y. Ching. 2021. "First-Principles Calculation of Lattice Distortions in Four Single Phase High Entropy Alloys with Experimental Validation," *Mater. Des.* 209, 1100712.

Sawan, M.E. 2014. "Transmutation of Tungsten in Fusion and Fission Nuclear Environments," *Fusion Sci. Technol.* 66, 272–277.

Snead, L.L., S.J. Zinkle, and D.P. White. 2005. "Thermal Conductivity Degradation of Ceramic Materials Due to Low Temperature, Low Dose Neutron Irradiation," *J. Nucl. Mater.* 340, 187–202.

Snead, L.L., Y. Katoh, and S. Connery. 2007. "Swelling of SiC at Intermediate and High Irradiation Temperatures," *J. Nucl. Mater.* 367, 677–684.

Was, G.S., Z. Jiao, E. Getto, K. Sun, A.M. Monterrosa, S.A. Maloy, O. Anderoglu, B.H. Sencer, and M. Hackett. 2014. "Emulation of Reactor Irradiation Damage Using Ion Beams," *Scripta Materialia* 88, 33–36.

Was, G.S. 2007. Chapter 3, "The Damage Cascade," in *Fundamentals of Radiation in Materials*—125–133, Springer, Berlin, Heidelberg, New York.

Was, G.S. 2007. Chapter 11: "Simulation of Neutron Irradiation Effects with Ions," *Fundamentals of Radiation in Materials,* 545–576, Springer, Berlin, Heidelberg, New York (2007).

Was, G.S., and T. Allen. 1994. "Radiation-Induced Segregation in Multicomponent Alloys: Effect of Particle Type," *Mater. Charact.* 32(4), 239–255.

Wigner, E.P. 1946. "Theoretical Physics in the Metallurgical Laboratory of Chicago," *J. Appl. Phys.* 17, 857–863.

Wu, Z., M.C. Troparevsky, Y.F. Gao, J.R. Morris, G.M. Stocks, and H. Bei. 2017. "Phase Stability, Physical Properties and Strengthening Mechanisms of Concentrated Solid Solution Alloys," *Curr. Opin. Solid State Mater. Sci.* 21, 267–284.

X-5 Monte Carlo Team. 2003. *MCNP—A General Monte Carlo N-Particle Transport Code, Version 5*, LA-CP-03-0245, Los Alamos National Laboratory.

Zhang, Y., Y.N. Osetsky, and W.J. Weber. 2022. "Tunable Chemical Disorder in Concentrated Alloys: Defect Physics and Radiation Performance," *Chem. Rev.* 122, 789–829.

Zhang, Y., C. Silva, T. G. Lach, M. A. Tunes, Y. Zhou, L. Nuckols, W. L. Boldman, P. D. Rack, S. E. Donnelly, L. Jiang, L. Wang, and W. J. Weber. 2022. "Role of Electronic Energy Loss on Defect Production and Interface Stability: Comparison between Ceramic Materials and High-Entropy Alloys," *Curr. Opin. Solid State Mater. Sci.* 26, 101001.

Zhang, Y., and W.J. Weber. 2020. "Ion Irradiation and Modification: Coupled Electronic and Nuclear Energy Dissipation and Subsequent Non-Equilibrium Processes in Materials," *Appl. Phys. Rev.* 7, 041307.

Zhang, Y., H. Xue, E. Zarkadoula, R. Sachan, C. Ostrouchov, P. Liu, X. lin Wang, S. Zhang, T.S. Wang, and W.J. Weber. 2017. "Coupled Electronic and Atomic Effects on Defect Evolution in Silicon Carbide under Ion Irradiation," *Curr. Opin. Solid State Mater. Sci.* 21, 285–298.

Zhang, Y., et al. 2014. "New Ion Beam Materials Laboratory for Materials Modification and Irradiation Effects Research," *Nucl. Instrum. & Meth. B* 338, 19–30.

Zhang, Y., T. Varga, M. Ishimaru, P.D. Edmondson, H. Xue, P. Liu, S. Moll, F. Namavar, C. Hardiman, S. Shannon, and W.J. Weber. 2014. "Competing Effects of Electronic and Nuclear Energy Loss on Microstructural Evolution in Ionic-Covalent Materials," *Nucl. Instru. and Meth. B* 327, 33–43.

Zinkle, S.J., V.A. Skuratov, and D.T. Hoelzer. 2002. "On the Conflicting Roles of Ionizing Radiation in Ceramics," *Nucl. Instrum. Methods Phys. Res. B* 191, 758–766.

Zinkle, S.J., and L.L. Snead. 2018. "Opportunities and Limitations for Ion Beams in Radiation Effects Studies: Bridging Critical Gaps between Charged Particle and Neutron Irradiations." *Scr. Mater.* 143, 154–160.

APPENDIX A. ADDITIONAL PLOTS SUPPORTING SECTION 4.1

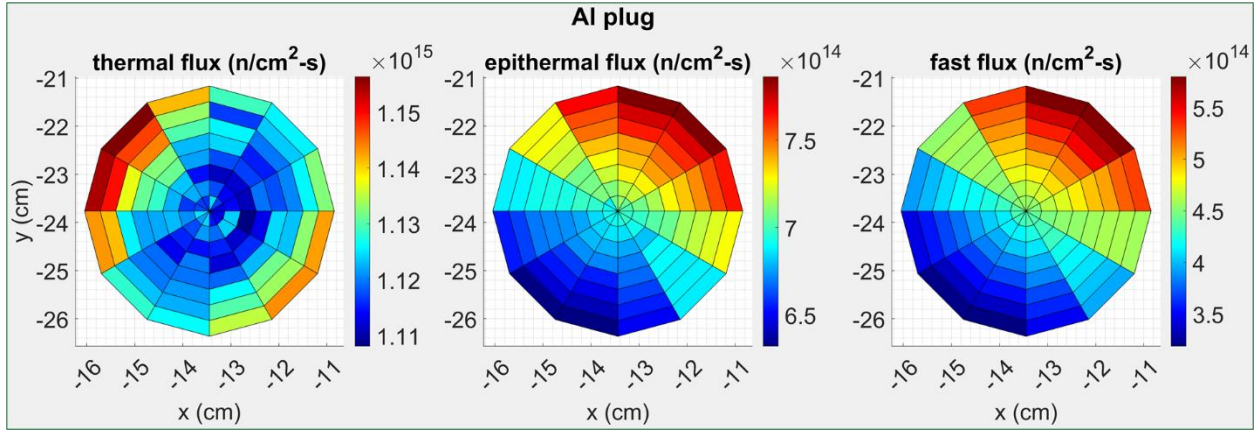# APPENDIX A. ADDITIONAL PLOTS SUPPORTING SECTION 4.1

Figure 17. Three-energy group neutron flux distribution in the Al plug configuration.
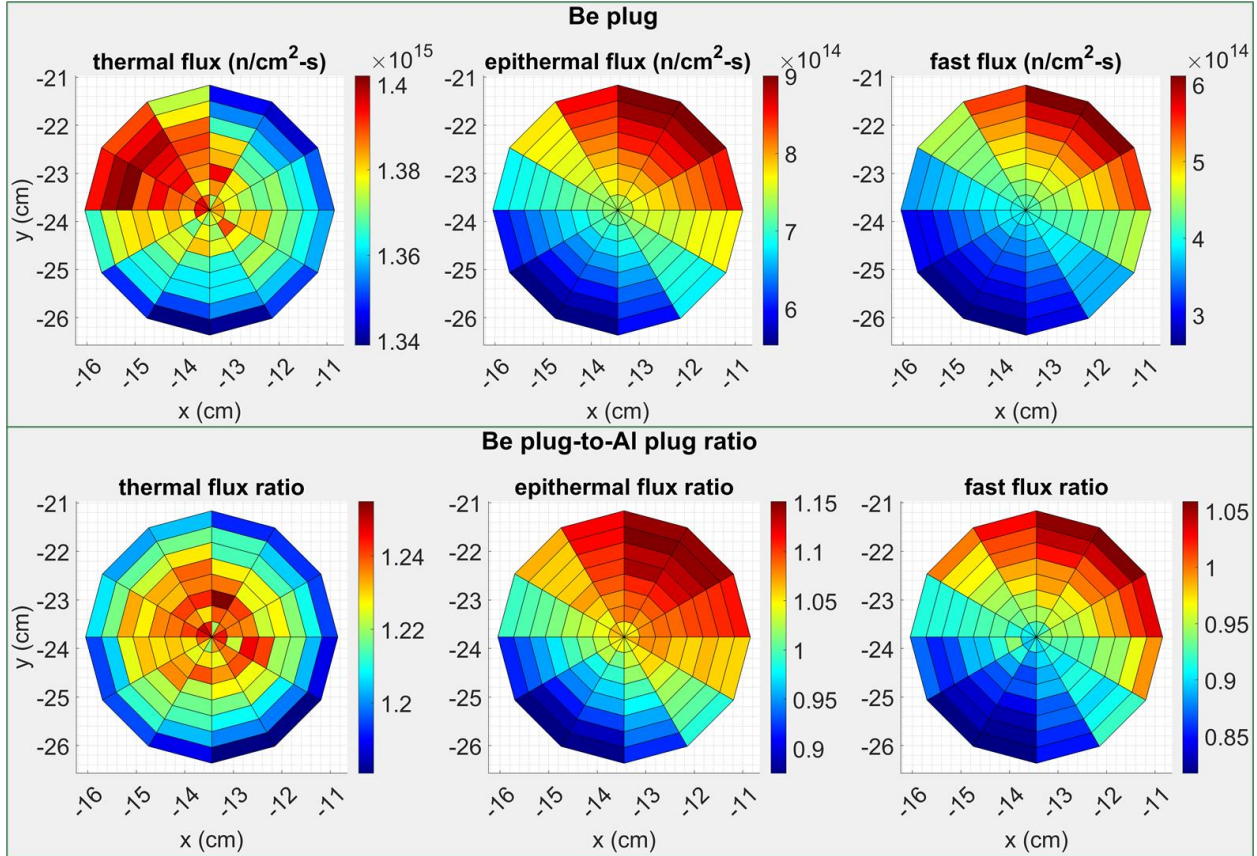

Figure 18. Three-energy group neutron flux distribution in the Be plug configuration and comparison to the reference Al plug configuration.
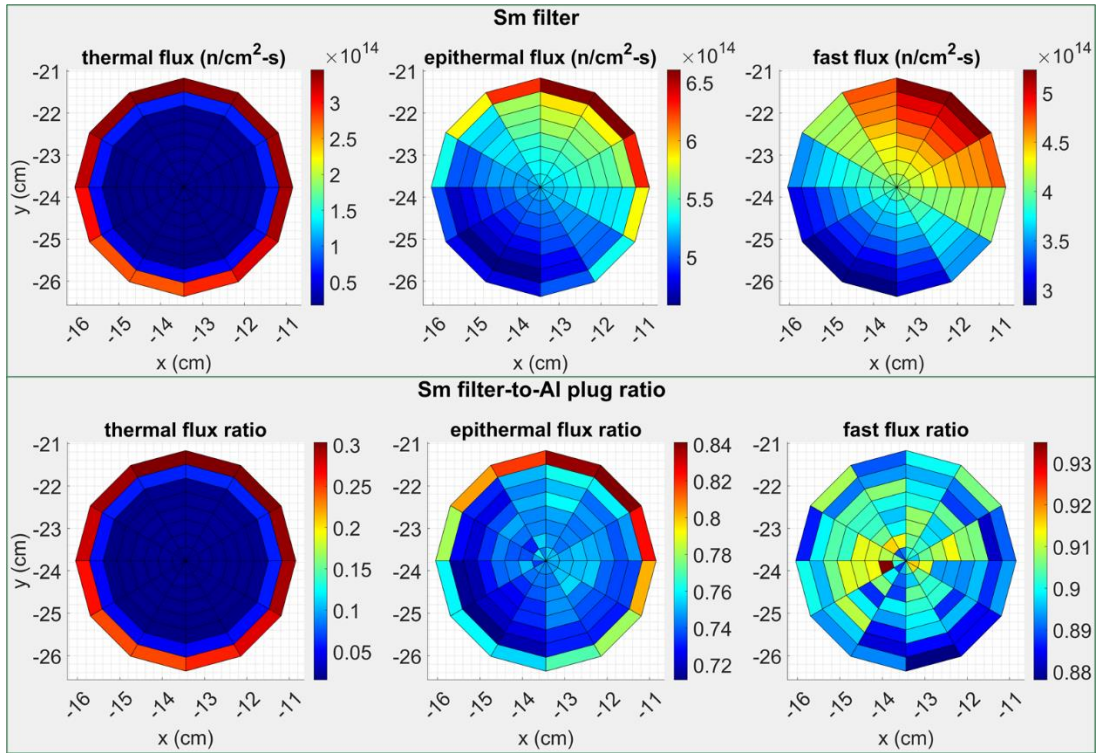
Figure 19. Three-energy group neutron flux distribution in the Sm poison filter configuration and comparison to the reference Al plug configuration.
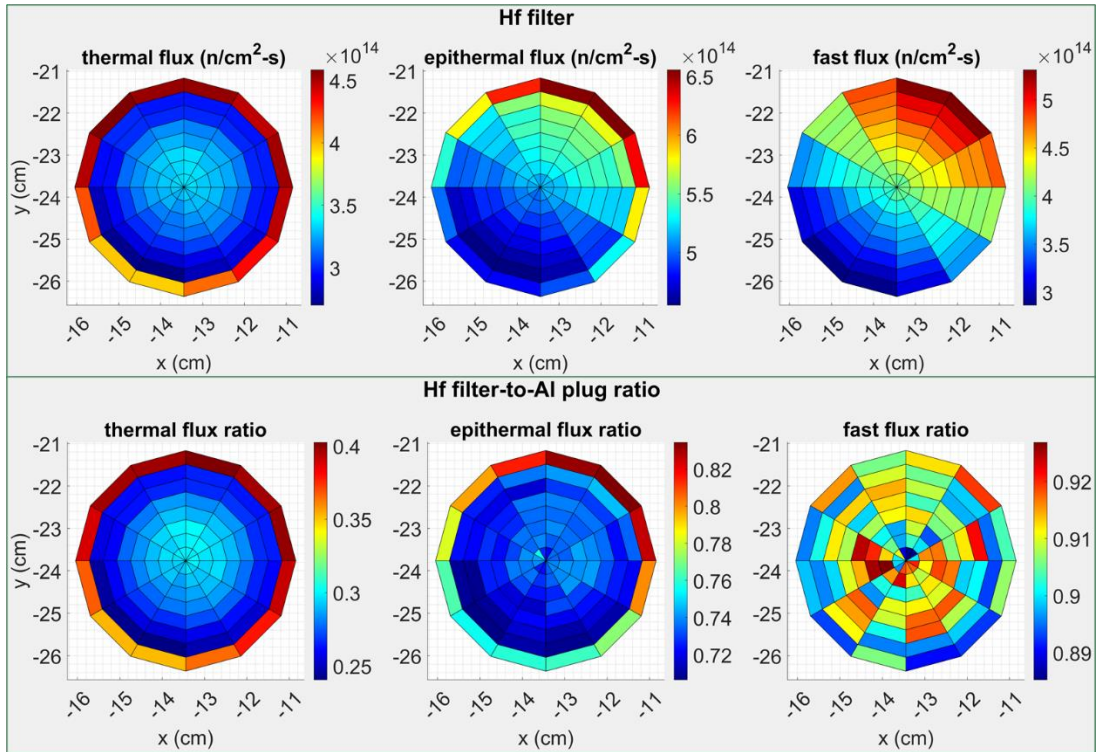
Figure 20. Three-energy group neutron flux distribution in the Hf poison filter configuration and comparison to the reference Al plug configuration.
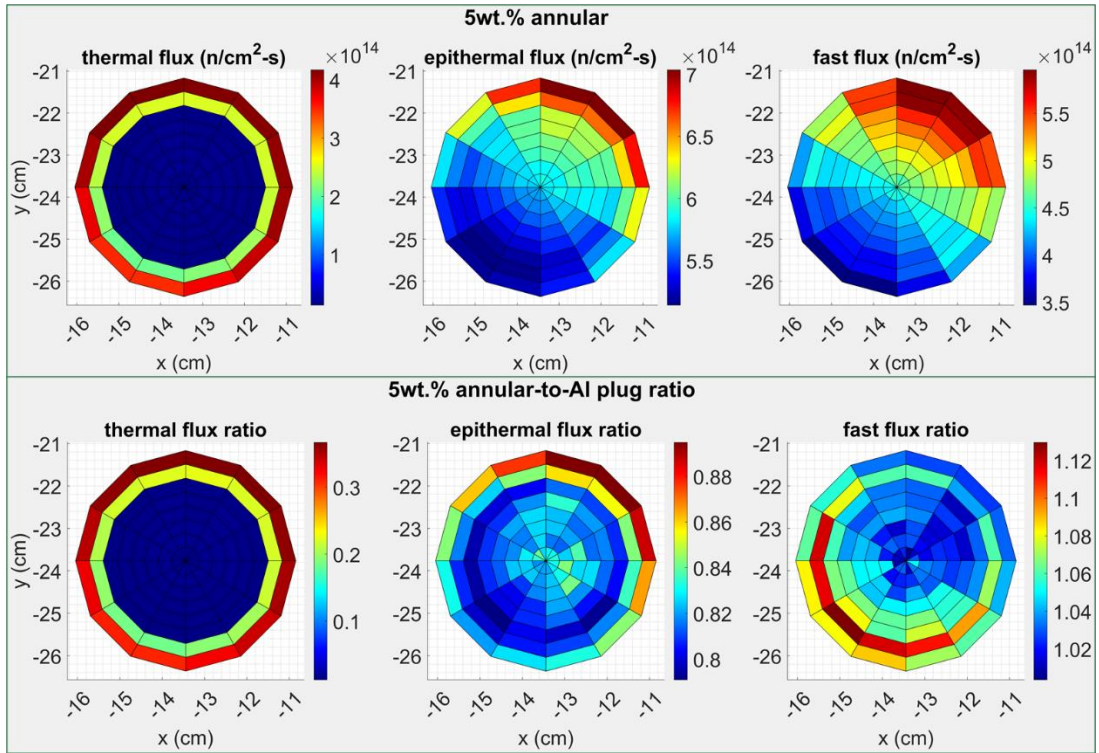
Figure 21. Three-energy group neutron flux distribution in the 5 wt% annular fast-flux booster plus Gd poison filter configuration and comparison to the reference Al plug configuration.

Figure 22. Three-energy group neutron flux distribution in the 10 wt% annular fast-flux booster plus Gd poison filter configuration and comparison to the reference Al plug configuration.

Figure 23. Three-energy group neutron flux distribution in the 15 wt% annular fast-flux booster plus Gd poison filter configuration and comparison to the reference Al plug configuration.
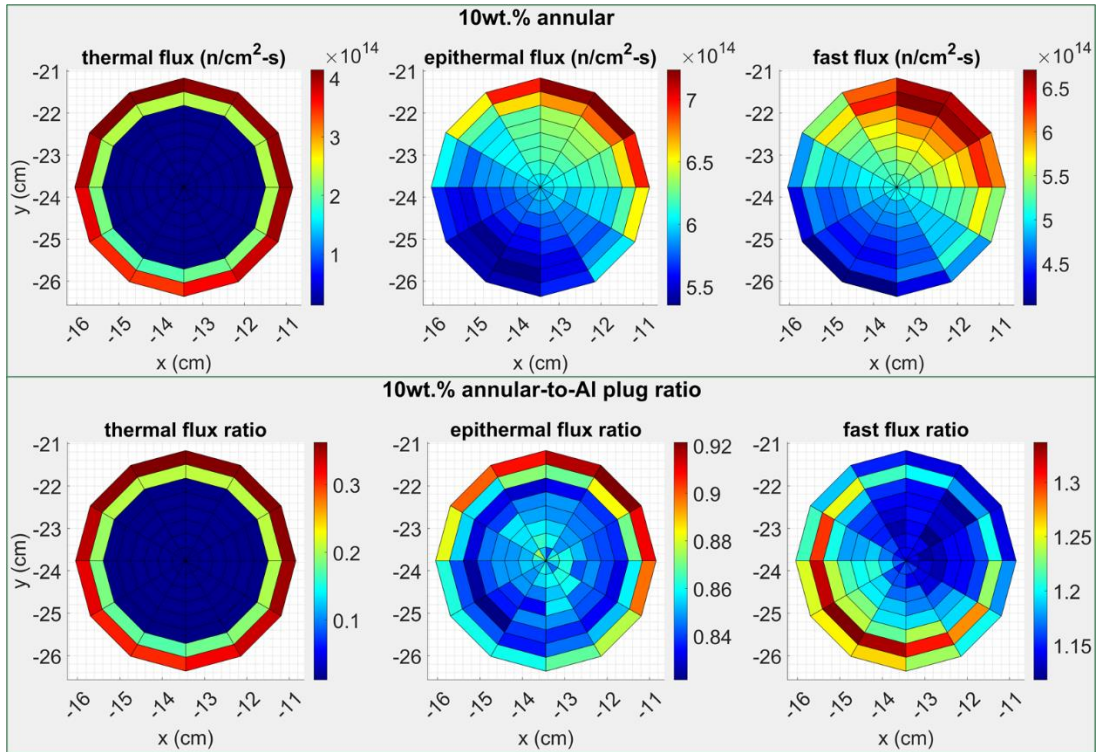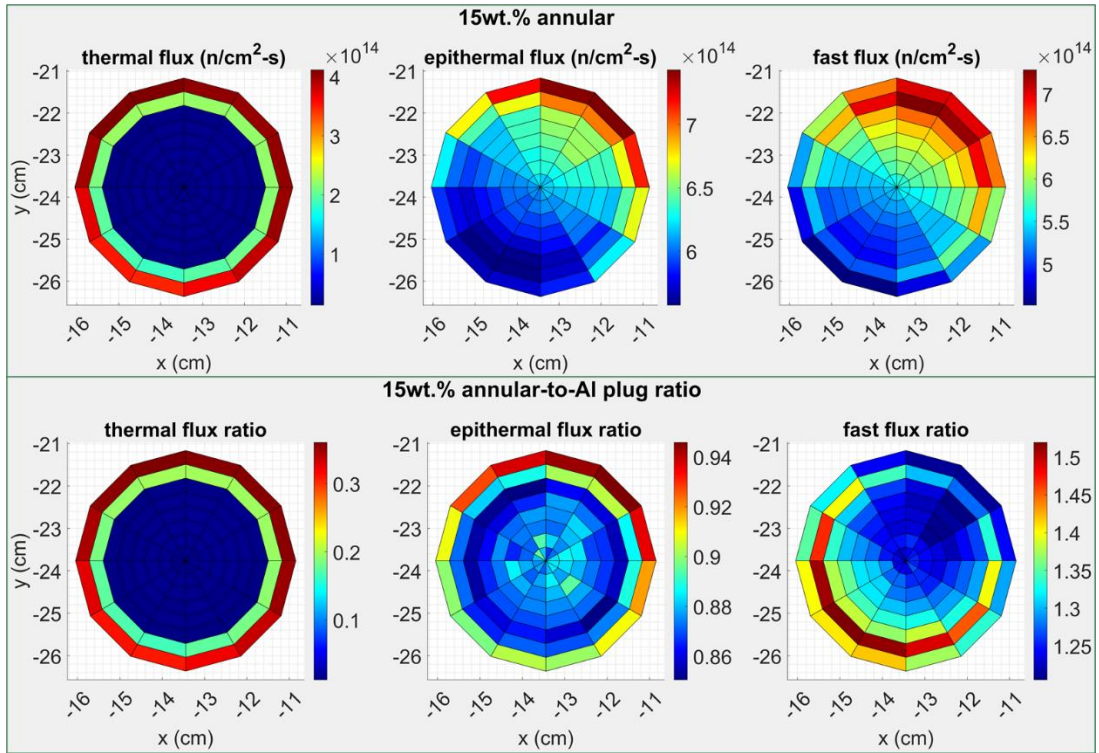

Figure 24. Three-energy group neutron flux distribution in the 5 wt% semi-circle fast-flux booster plus Gd poison filter configuration and comparison to the reference Al plug configuration.

Figure 25. Three-energy group neutron flux distribution in the 10 wt% semi-circle fast-flux booster plus Gd poison filter configuration and comparison to the reference Al plug configuration.
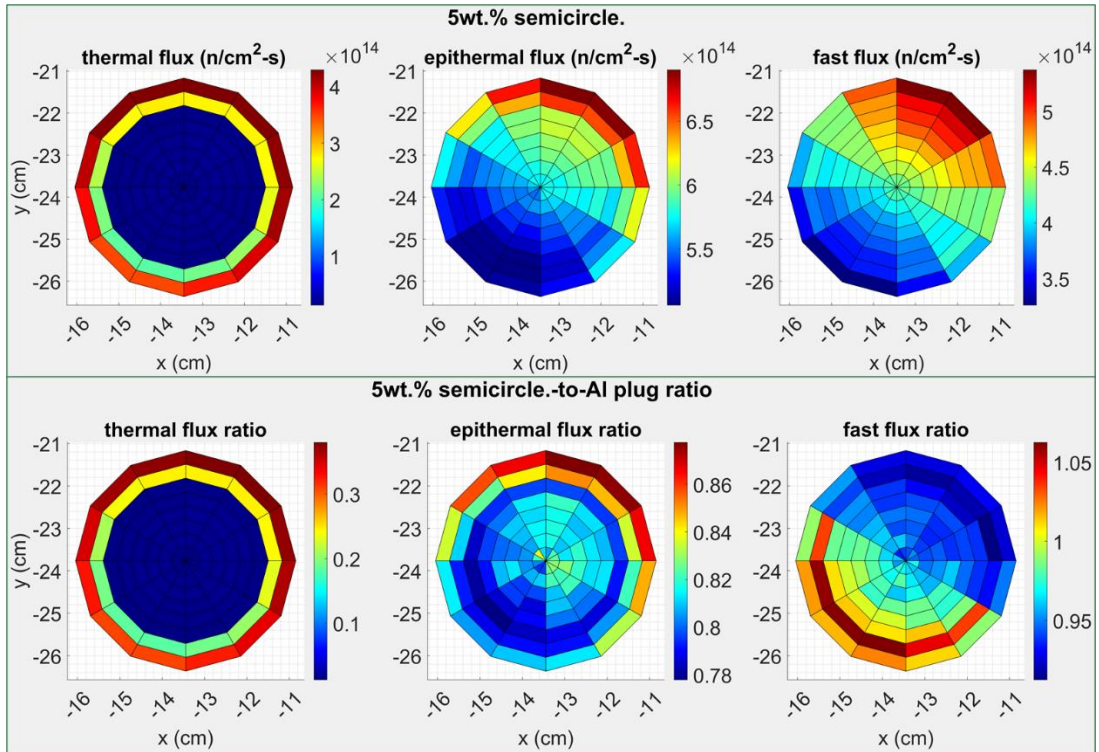

Figure 26. Three-energy group neutron flux distribution in the 15 wt% semi-circle fast-flux booster plus Gd poison filter configuration and comparison to the reference Al plug configuration.
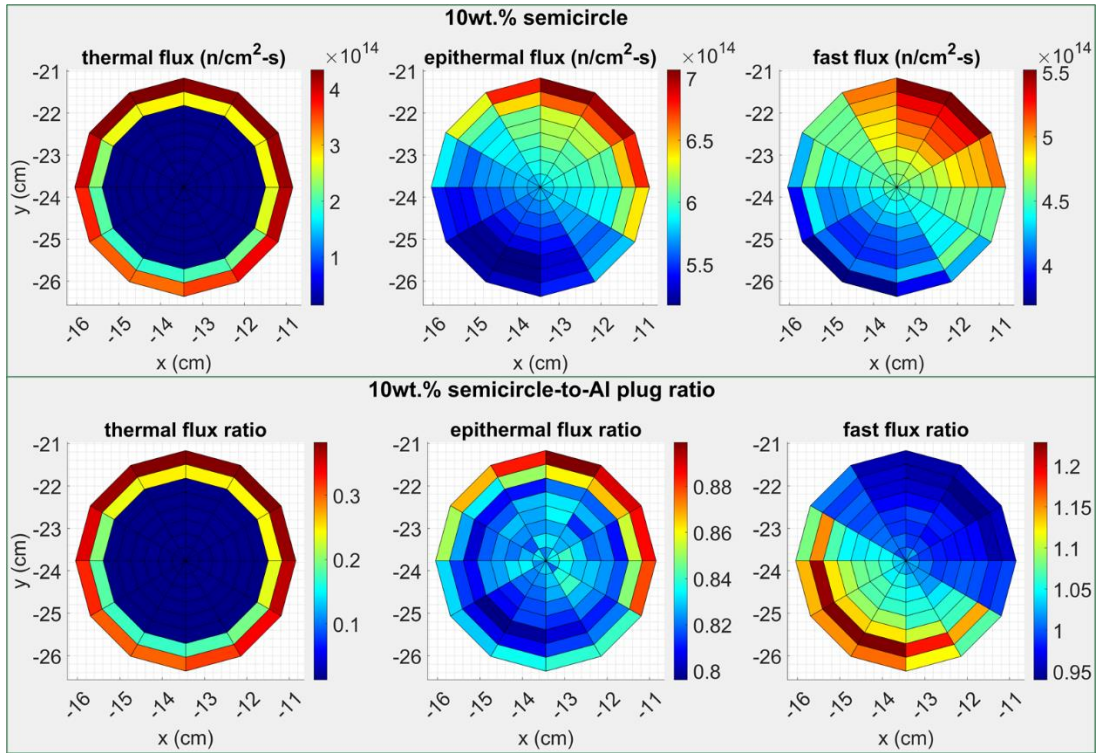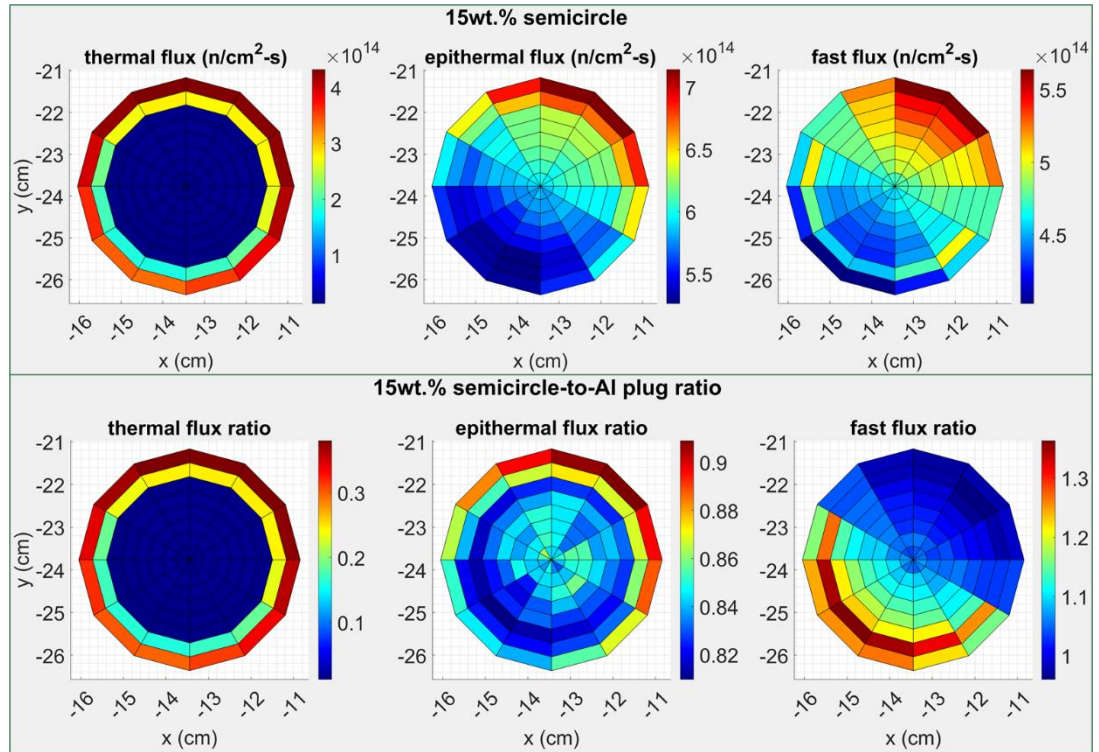
APPENDIX B. SUPPORTING ION BEAM FACILITY EXAMPLES

APPENDIX B. SUPPORTING ION BEAM FACILITY EXAMPLES

B.1. EXAMPLE OF ION IRRADIATED SIC

For neutron-irradiated SiC, an equivalence of 1×10^{25} n m^{-2} (E > 0.1 MeV) = 1 dpa was adopted in some experimental research (Snead 2005, Snead 2007, Katoh 2013). This equivalence is sensible when damage by neutron irradiation is compared because of the overwhelming majority of the displacement damage produced by fast neutrons (> 0.1 MeV). Nonetheless, if damage by neutrons is compared to that by heavy ions, then differences arising from the above *four fundamental aspects* must be addressed. Particular challenges are the athermal effects (Zhang 2020) from hot electrons created along the trajectory of ions vs. neutron-generated PKAs, as well as differences in recoil spectra and cascade density on damage evolution.

Neutron spectra for some typical material test reactors (Guo 2016) are presented in Figure 27. Because applications of SiC have been proposed for both fission and fusion reactors, spectra of a typical PWR and a DEMO (DEMOnstration fusion power plant) reactor with helium-cooled pebble bed blanked form, respectively, are also included. In addition, because structural materials for the fusion DEMO reactor are due to be irradiated in the International Fusion Materials Irradiation Facility (IFMIF), the neutron spectrum in the High Flux Test Module (HFTM) in IFMIF is also considered (Guo 2016).
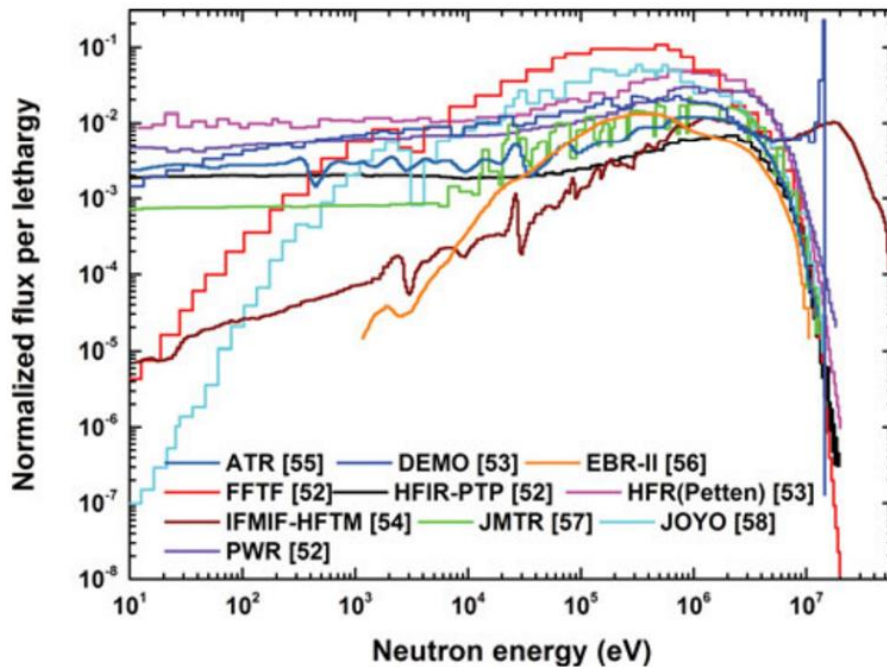

Figure 27. Neutron spectra for some typical material test reactors (Guo 2016). Includes the center flux trap of ATR [55], DEMO with helium-cooled pebble bed blanket [53], EBR-II [56], FFTF mid core [52], the mid-plane of the peripheral target position (PTP) of HFIR [52], HFR (Petten) [53], IFMIF-HFTM [54], fuel area of JMTR [57], core center of JOYO [58], and PWR [52].

Figure 28 presents the primary recoil spectra induced in SiC by three different projectiles: 150 keV Ne, 800 keV Bi ions, and neutron flux of a high-temperature reactor (HTR). The analysis of the primary recoil spectra (Figure 28, left) clearly shows that heavy ions are not able to produce a primary recoil spectrum like that produced in an HTR. However, the weighted recoil spectra induced by 800 keV Bi ions and neutrons produced in an HTR are more alike (Figure 28, right). This analysis clearly shows that *ion accelerators can at least qualitatively simulate radiation damage induced by nuclear reactors*. It is noted

that the difference in W(T) between the various types of irradiations is evident (Was 2007). Whereas heavy ions come closer to reproducing the energy distribution of recoils of neutrons than do light ions, neither is accurate in the "tails" of the distribution. This does not mean that ions are poor simulations of radiation damage, but it does mean that damage is produced differently and that this must be considered when assessing the microchemical and microstructural changes caused by irradiation.
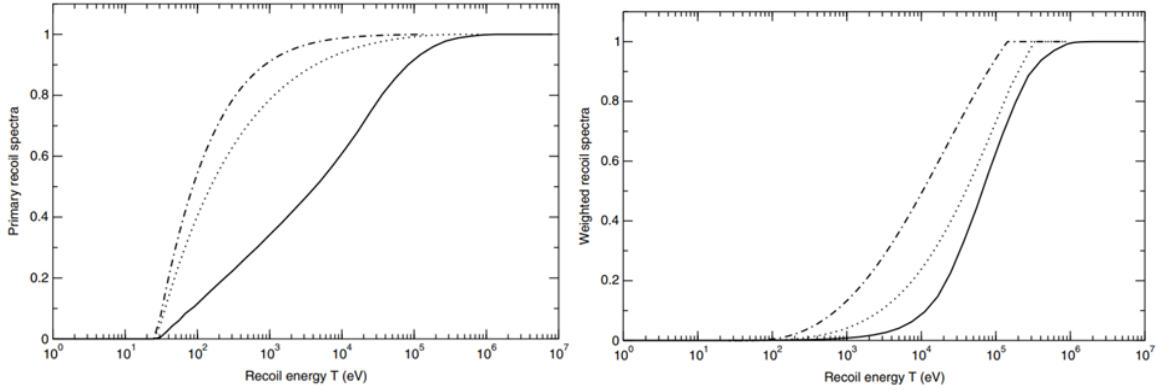

Figure 28. Primary recoil spectra (left) and weighted recoil spectra (right) induced in SiC by 150 keV Ne (dashed-dotted line), 800 keV Bi ions (dotted line) and neutron flux of HTR (solid line) (Lunéville 2016). These primary recoil spectra are different, but the weighted recoil spectra are less different.

In another study, the effects of recoil spectra and ratio of total ionization energy to damage energy dissipation are investigated in 3C-SiC single crystals by comparing defect survival from 10 MeV Au ions with self-ion irradiation using 5 MeV Si ions. The 10 MeV Au and 5 MeV Si ions have comparable pathlengths and electronic energy loss values, as shown in Figure 29. Whereas self-ion irradiations are generally recommended, nuclear energy loss and damage energy for the 5 MeV Si ions are significantly lower than for 10 MeV Au ions. By comparing measured rates of disorder accumulation at different depths (Figure 29), the effects of recoil spectra and the total ionization-to-damage energy ratio can be evaluated based on predicted weighted recoil spectra (Figure 30) and radial dissipation of ionization and damage energy (Figure 31).
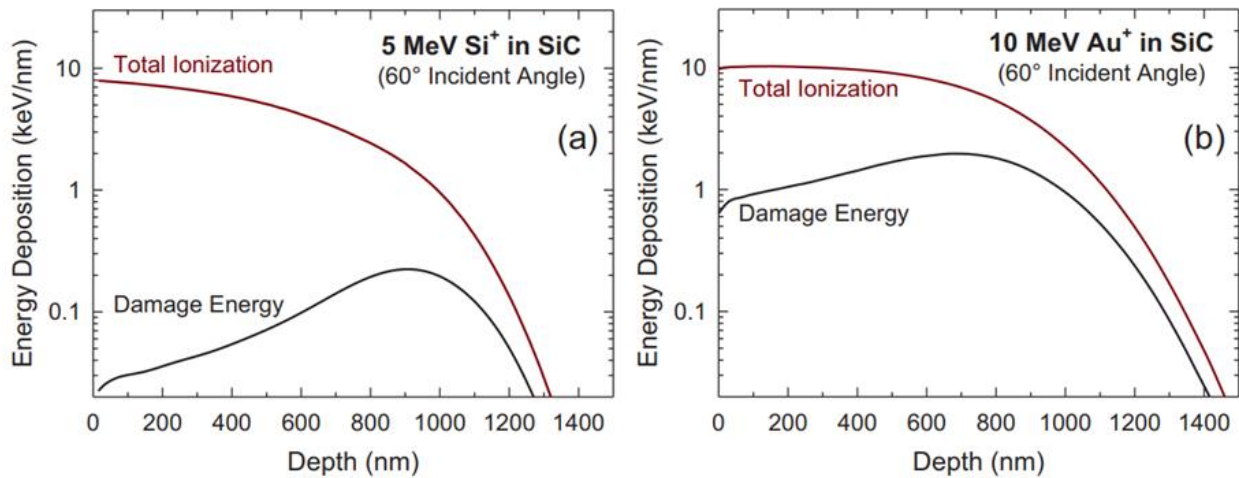

Figure 29. The partitioning of incident ion energy (per unit depth) to total ionization energy (inelastic energy transfer to electrons by the incident ion and secondary recoils) and to the damage energy (elastic energy going into atomic displacements): (a) 5 MeV Si ions in SiC at an incident angle of 60°; and (b) 10 MeV Au ions at an incident angle of 60° (Nuckols 2021).
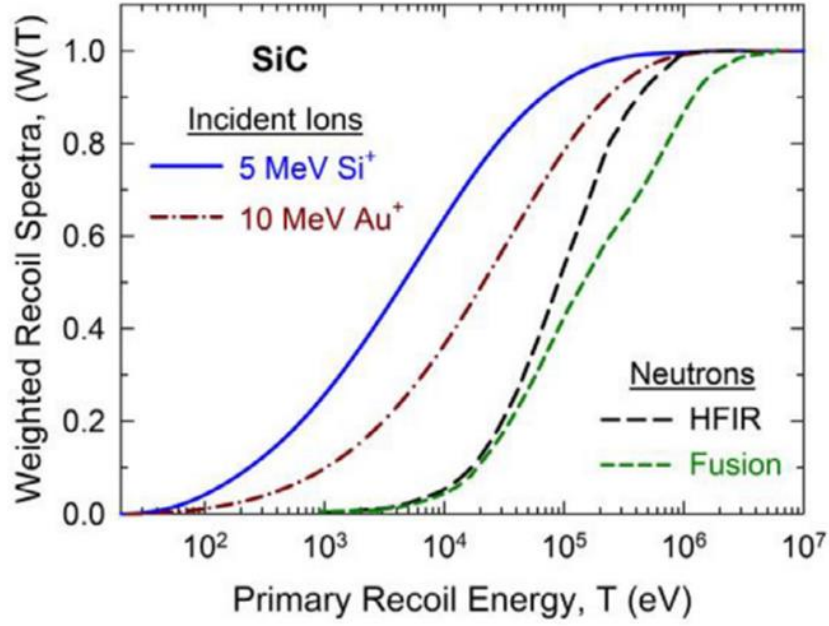
Figure 30. Weighed primary recoil spectra for 5 MeV Si and 10 MeV Au ions in SiC (Nuckols 2021)and for neutron irradiations in HFIR and a fusion reactor (Guo 2014).
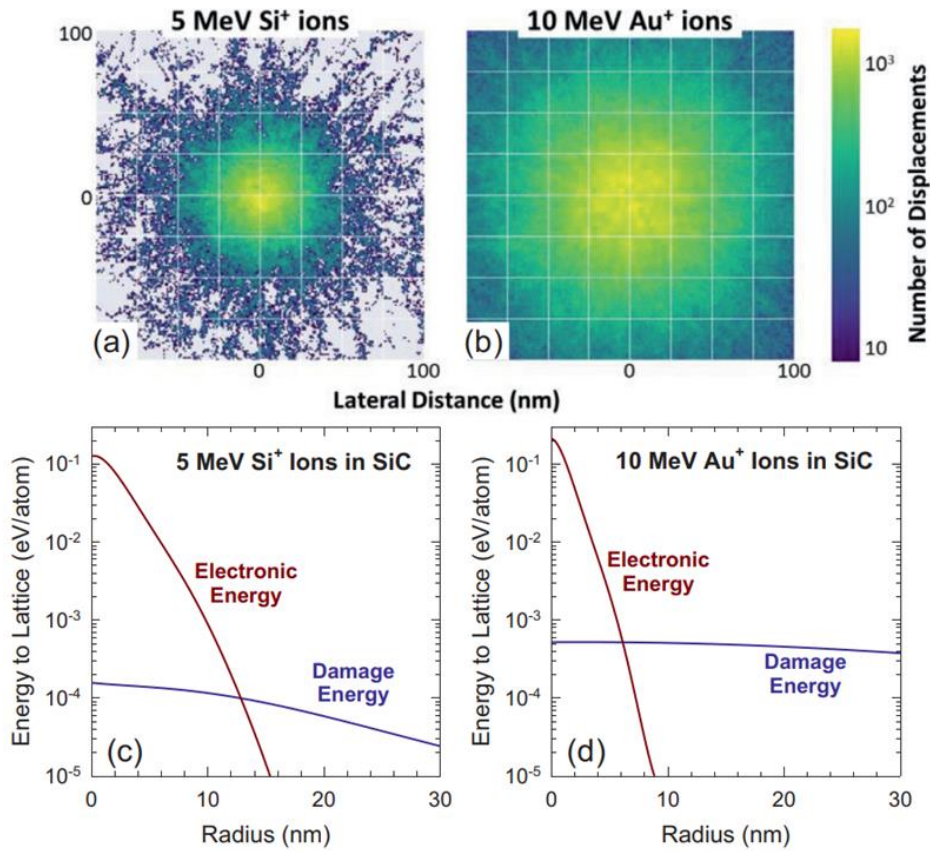
Figure 31. Radial distribution of displacement collisions by full-cascade SRIM simulations along a segment of pathlength from 700 to 800 nm predicted for (a) 5 MeV Si ions and (b) 10 MeV Au ions; electronic (ionization) and damage energy deposited to the atomic lattice over a pathlength of 700 to 800 nm by (c) 5 MeV Si ions and (d) 10 MeV Au ions (Nuckols 2021).

B-5

The weighted recoil spectra for 5 MeV Si and 10 MeV Au ions in SiC are shown in Figure 30, along with the weighted recoil spectra in SiC for HFIR neutrons and a fusion reactor (Guo 2014). A major effect of the lower damage energy for the 5 MeV Si ions shown in Figure 29 (a) is a softer primary recoil energy spectrum than that for 10 MeV Au ions (Figure 30). The primary recoil spectra for 5 MeV Si and 10 MeV Au ions were determined by using Pysrim (Ostrouchov 2018) to examine the full cascade collision files created by the SRIM 2008 code for 10,000 incident ions of each type. As discussed above, whereas the primary recoil spectrum for a given ion is important, a more meaningful measure of the overall effect of recoil spectrum on defect production is the weighted primary recoil spectrum, W(T), which is the fraction of displaced atoms produced by all primary recoils with energies less than that of a given primary recoil energy (Averback 1994). It can be seen in Figure 30 that recoils produced from Si and Au ions are weighted toward lower energies because of the screened Coulomb potential that controls the interactions of charged particles. For an unscreened Coulomb interaction, the probability of creating a recoil of energy T varies as $1/T^2$. Because neutrons interact as hard spheres, the probability of a creating a recoil of energy T is independent of recoil energy (Was 1994, Was 2007). Like the results shown in Figure 28 (right), the large difference in W(T) is noticeable between the Si and Au irradiations and between the ions and neutrons, especially in the "tails" of the distribution (Was 2007). The differences suggest that damage is produced differently, which must be considered when assessing the microchemical and microstructural changes due to irradiation, as noted above (Was 2007).

Radial distribution of displacement collisions along a segment of ion paths is predicted in Figure 31 for 5 MeV Si ions (a) and 10 MeV Au ions (b), respectively. The radial dissipation of damage energy along the ion pathlength for incident ions cannot be estimated directly from the SRIM full-cascade collision files. To determine this, the radial distributions of displacements for 5 MeV Si and 10 MeV Au are first ascertained using Pysrim to examine 10,000 full-cascade collision files created by the SRIM code for each ion type over the pathlength segment from 700 to 800 nm (corresponding to a depth from 350 to 400 nm for an incident angle of 60°), as seen in Figure 29. These radial distributions of displacements are illustrated in Figure 31, and the significant greater radial extent of displacements from 10 MeV Au ions is caused by the harder primary recoil spectrum for Au ions compared to Si ions over this depth range (Figure 29). The results further reveal that coupling between ionization and damage energy dissipation for the Si ions is stronger (Figure 31a), and therefore defect survival along the ion trajectory is more sensitive to changes in ionization energy. In contrast, the more energetic recoil spectra resulting from the 10 MeV Au ions leads to weaker spatial coupling of inelastic and elastic process (Figure 31b).

To better understand the coupling of ionization energy and damage energy along the actual trajectory or pathlength of an ion, the radial dissipation of both the ionization energy and the damage energy to the atomic structure were examined, as shown in Figure 31c and d. Using the total integrated number of displacements and the integrated damage energy (Figure 29) from full-cascade simulations for each ion, the average amount of damage energy deposited per displacement event has been determined and used to estimate the radial dissipation of damage energy from the radial distribution of displacements for each ion. The radial distributions of damage energy (eV/atom) are shown in Figure 31c and d. The ionization energy deposited by an incident ion of specific energy to the target electrons along an incremental ion pathlength is given by the electronic stopping power (energy deposition per unit pathlength), which creates a high density of hot electrons that dissipate their energy to the atomic structure via electron-phonon coupling, leading to a highly localized thermal transient along the ion pathlength. This transient is generally referred to as the *inelastic thermal spike*, which has a duration of tens of ps to several hundred ps. The radial profile of electronic energy dissipation density to the lattice by 5 MeV Si and 10 MeV Au ions in SiC over the segment of pathlength from 700 to 800 nm has been calculated based on the two-temperature model and model parameters described previously for SiC (Zhang 2017). The results are included in Figure 31c and d. The coupling (i.e., overlap) of electronic energy and damage energy along the ion pathlength occurs over a much larger radius and with a much higher ratio of electronic-to-damage energy for the 5 MeV Si ions compared to that of the 10 MeV Au ions, which can result in decreased

defect survival along the ion trajectory for the Si ions. The study of SiC irradiated using 10 MeV Au ions shows more damage survival at similar doses, and it also shows significantly reduced (by a factor of 20 or more) implanted ion concentrations compared to the results from the 5 MeV Si irradiations.

B.2. EXAMPLE OF ION IRRADIATED NANOCRYSTALLINE HIGH-ENTROPY ALLOYS

High-entropy alloys (HEAs) and some complex alloys exhibit desirable properties and significant structural stability in harsh environments. To address the abundant challenges in developing structural alloys for next-generation nuclear power systems, the promising properties resulting from the tunable chemical complexity in concentrated solid-solution alloys (CSAs), including HEAs, have recently attracted increased attention (Zhang 2021, Pickering 2021). In this example, Ni self-ions and heavier Au ions with energies of up to 23 MeV were chosen to deposit electronic (ionizing) and damage energy into nanocrystalline HEAs—equiatomic $Ni_{20}Fe_{20}Co_{20}Cr_{20}Cu_{20}$ (HEA-20Cu) and non-equiatomic $(NiFeCoCr)_{97}Cu_3$ (HEA-3Cu) films. The aim of using different ion masses and energies was to deposit ionizing energy and ballistic energy at different rates and ratios to (1) target electrons and nuclei, respectively, and (2) to discuss the *four fundamental aspects*.

Here, the nanocrystalline HEA-3Cu and HEA-20Cu films are chosen to especially reveal ionization effects (*Aspect 4*). It is known that $Ni_{25}Fe_{25}Co_{25}Cr_{25}$ (NiFeCoCr) is a single-phase face-centered cubic (fcc) solid solution with a greater reduced thermal conductivity than of pure Ni or Fe resulting from alloying element Cr. Furthermore, alloying with Cu stabilizes the crystalline structure to form fcc HEA-3Cu and HEA-20Cu. Nevertheless, due to the positive enthalpy of mixing with other alloying constituents and the tendency of phase separation, an additional fcc phase with local concentration variation may form (Wu 2017, San 2021), especially during thermal treatment or under irradiation. Chemical complexity does not monotonically increase with the number of alloying elements; it depends on the coupling strengths of constituents (i.e., electron, magnetic, and phonon interactions) (Zhang, 2021). Therefore, the maximum chemical complexity may not occur at the maximum compositional disorder, which is the equiatomic composition. In equiatomic HEA-20Cu, there are 40% of Cr+Fe and 60% of Co+Ni+Cu, whereas in nonequiatomic HEA-3Cu, the corresponding percentages are 48.5% and 51.5%, respectively. Because of relatively lower Cr and Fe concentrations, 20% each, in HEA-20Cu, slightly reduced differences exist between the partially filled and fully filled *d* orbitals. In HEA-3Cu, the difference is greater, so the chemical complexity is expected to be slightly higher, and the electronic effects may be more noticeable. These intrinsic properties, together with dense interfaces and GBs in their nanocrystalline form, make the alloys a good model system to demonstrate the non-negligible effects of ionization.

The weighted recoil spectrum for Ni and Au ions within the first micrometer in the HEA-20Cu film is shown in Figure 32. The weighted recoil spectra suggest that about 50% of the displacements are produced by PKAs with energies of less than 40 keV for Ni ions and less than 125 keV for Au ions. Clearly, harder recoil spectra (i.e., higher recoil energies) are observed for the Au ions over the film thickness. The relatively softer recoil spectra from the Ni irradiation produce fewer and more isolated simple defects in the cascade events. In the case of 23 MeV Au irradiation, the weighted recoil spectrum shows that the PKAs extends to primary recoil energies that are higher than the spectrum for 11 MeV Au irradiation.
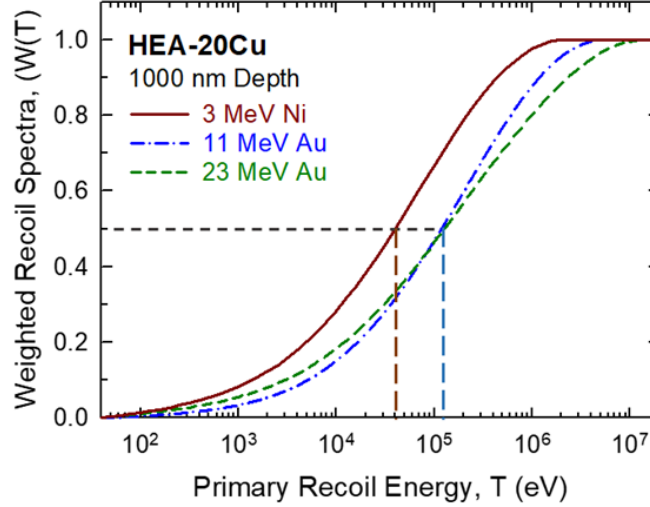
Figure 32. Weighted recoil spectra for Ni and Au ions within the first micrometer in the HEA-20Cu film. Long-dashed lines indicate the PKA energy below which ~50% of the displaced atoms are produced (Zhang 2022).

To evaluate whether the microstructural instability results mainly from direct displacement collisions (E_{damage}) and if the contribution from ion energy transfer to electrons ($E_{ionization}$) is negligible, irradiation-induced growth as a function of integrated E_{damage} and E_{total} in the HEA-3Cu films is compared in Figure 33. The crystallite sizes determined using both the W–H plot (left column) and the Scherrer equation (right column) are summarized and compared. Noteworthy clustering of the data points is observed when the crystallite size is plotted as a function of integrated E_{total} (Figure 33b and d), as is clearly reflected by the increase in r^2 from 0.66 to 0.80, based on the W–H approach, and from ~ 0.36 to ~0.64 and 0.68 by fitting to the Scherrer equation. The notable clustering of the data points in Figure 33 when $E_{ionization}$ is considered suggests that energy transfer to target electrons has a significant impact on microstructural evolution and leads to effective grain growth. The contribution from ion energy transfer to electrons cannot be ignored, and analysis of such coupled energy dependences (E_{damage} and $E_{ionization}$) should provide insights into the particle-solid interaction processes (Zhang 2022).

A clearer perspective of the effect of different ions and energies can be obtained from the radial distributions of defect production from PKA cascades along an incremental depth of ion trajectories (Figure 34), as shown in Figure 31a and b for SiC. Whereas the radial distribution of displaced atoms from 23 MeV Ni ions is comparable to the initial crystallite size, the radial displaced atom distributions for all other ions are much larger than the initial crystallite sizes. When comparing the two radial distributions in Figure 34e and f, it can be seen that displaced atoms are more clustered along the trajectory of 23 MeV Au, which promotes strong spatial coupling of the inelastic thermal spike with atomic displacement processes. The wider radial spread of displaced atoms from 11 MeV Au ions leads to relatively weaker spatial coupling of electronic and atomic displacement processes (i.e., elastic thermal spikes).

To evaluate the grain growth in HEA-3Cu and HEA-20Cu induced by different ions, the crystallite size is plotted as a function of ion fluence in Figure 33 for all six irradiation conditions. When E_{damage} and $E_{ionization}$ are sizable and the contributions are entangled as the case in HEA-20Cu, the microstructural evolution may be revealed by plotting the crystallite size as a function of ion fluence (Figure 35). Temporal and spatial coupling of energy deposition processes from electrons and recoiling atoms control defect production and grain growth. Further research is required to reveal and quantify the correlation between the coupling strength and damage production or structure instability.
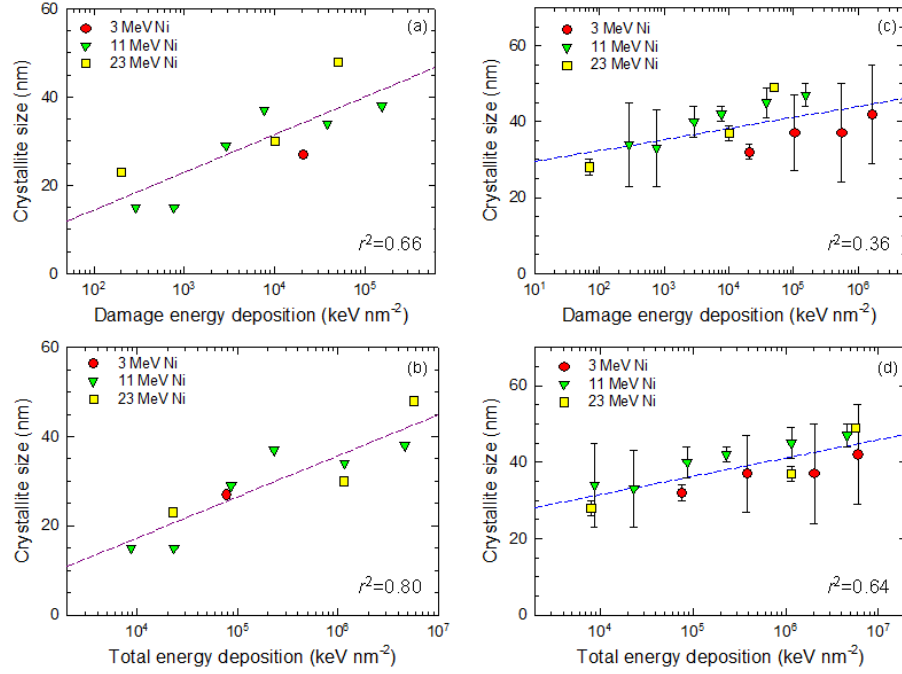
Figure 33. Ni irradiation-induced growth of crystallites in HEA-3Cu film (Zhang 2022) determined using the W–H method (left: a and b) and Scherrer formula from the (111) diffraction peak (right: c and d). The estimated crystallite size is plotted as a function of E_{damage} (a and c) and E_{total} (b and d). Dashed lines are the linear regression, and the coefficient of determination (r^2) is the square of the correlation as marked at the individual plots.
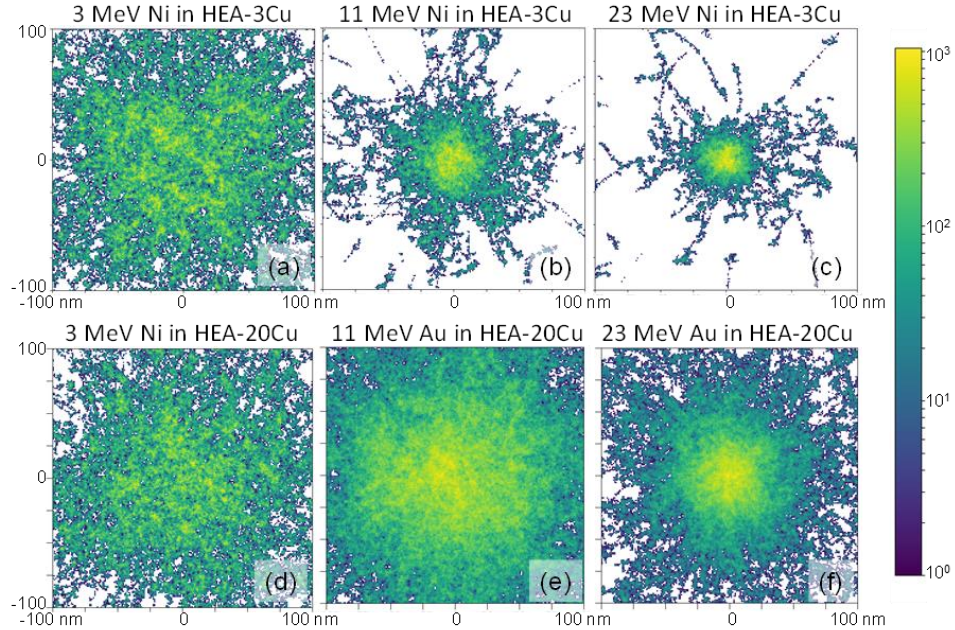

Figure 34. Distribution of displaced atoms from Pysrim based on SRIM full damage cascade simulations for 1000 ions penetrating an HEA-3Cu film (top: a, b, and c) and HEA-20Cu film (bottom: d, e and f) over a depth range of 450 to 550 nm, respectively (Zhang 2022). The irradiation condition is specified at the top of each plot.
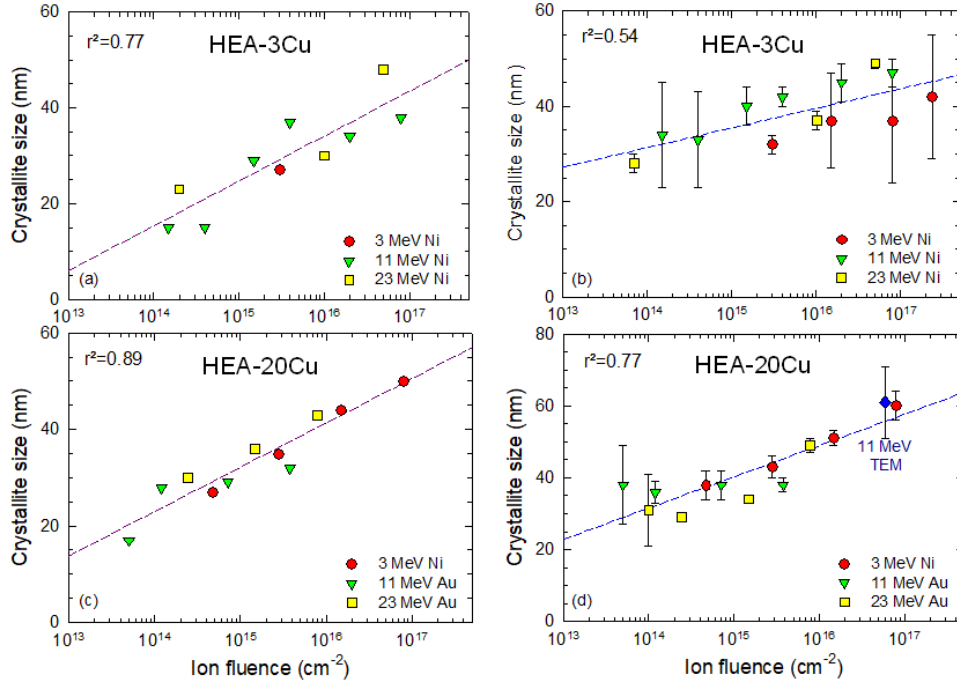
B-9

Figure 35. Crystallite size in HEA-3Cu (top: a and b) and HEA-20Cu (bottom: c and d), determined using the W–H method (left: a and c) and Scherrer formula (right: b and d), as a function of ion fluence (Zhang 2022). The dashed lines are the linear regression. Also included in (d) is the grain size determined from TEM images after 11 MeV Au irradiation to 5.98×10^{16} cm^{-2}. The coefficient of determination (r^2) is marked at the top left of the individual plots.

B.3. EXAMPLE OF NEUTRON AND IRRADIATED METALS

In the example shown in Figure 36, the weighted PKA energy values in copper for several irradiation species (e.g., 1 MeV neutrons, protons, Ne and Kr ions) are compared. Figure 37 illustrates the effect of the neutron flux on recoil spectra (Lunéville 2006). The total primary (left) and weighted recoil (right) spectra associated with neutron ^{93}Nb interactions are plotted vs. the recoil energy of ^{93}Nb atoms for PWR, FRB and HTR. Increasing the number of neutrons with a kinetic energy above 100 keV leads to a shift towards high kinetic energy of the primary recoil spectrum. This effect is less important for the weighted recoil spectrum because the number of displaced atoms are of the same order of magnitude for all reactors (Figure 37 right). In other words, the nature of the neutron flux drastically modifies the shape of the primary recoil spectra, but the weighted recoil spectra are not largely modified by the neutron fluxes.
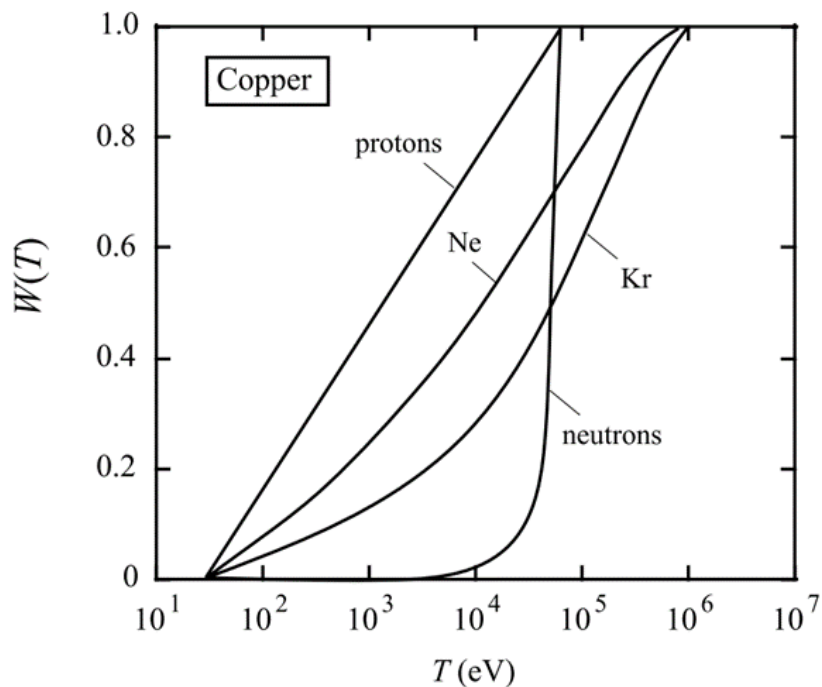
Figure 36. Weighted recoil spectra for 1 MeV particles in copper plotted as a function of recoil energy (T) (Was 2007, Averback 1994). Note the change in the weighted average recoil atom energies.
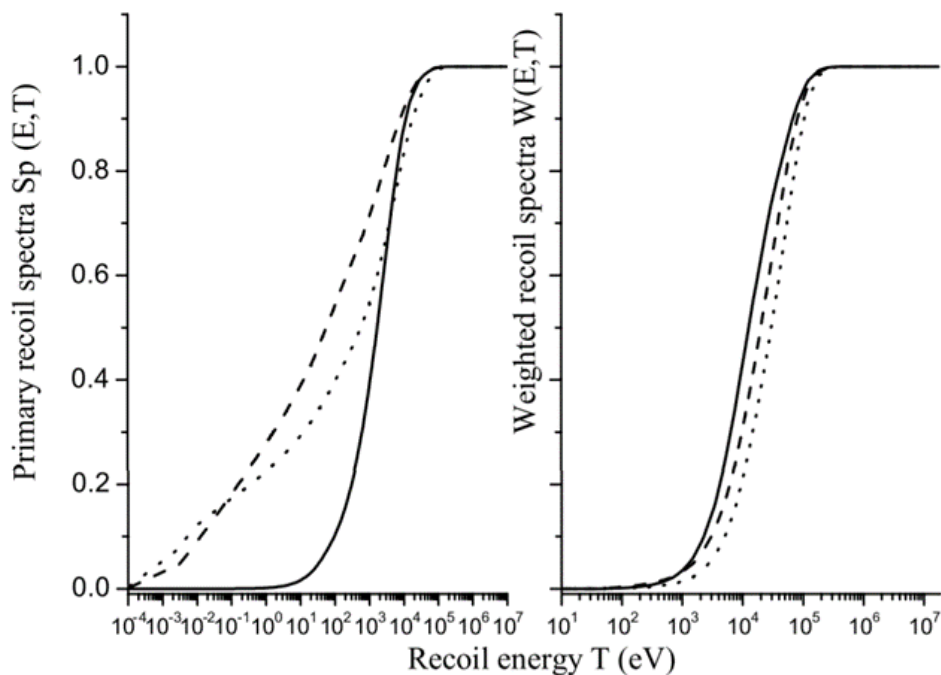

Figure 37. Comparison of primary recoil spectra and the weighted recoil spectra induced by 1 MeV neutron on ^{93}Nb with typical neutron fluxes produced in HTR (dashed line), PWR (dotted line) and FBR (solid line) (Lunéville 2006).

B.4. EXAMPLE OF SPECTRUM TAILORING BY ENERGETIC PROTONS (10+ MEV)

In a recent publication (Jepeal 2021), intermediate energy proton irradiation, using beams of 10–30 MeV protons, is evaluated for rapid high-fidelity materials testing for fusion and fission energy systems. Such protons have been identified as a uniquely flexible tool for studying radiation damage for nuclear power technology.

Several weighted recoil spectra for tungsten (Jepeal 2021) are plotted in Figure 38, both as cumulative distribution functions (top) and as probability distribution functions (bottom). Because of the widespread in neutron recoil energies shown from the fusion neutron spectrum and the fast breeder spectrum, intermediate-energy (10 MeV) protons have recoil spectra similar to that of the fusion and fast fission reactor cases. The work shows that intermediate energy protons can create recoils that are uniformly distributed across the range of recoils expected in fission and fusion reactors (up to 100 eV – 300 keV). They conclude that recoil energies produced by these protons are matched to those of fission and fusion reactor neutrons, ensuring similar radiation damage cascades and primary damage production. Lower energy protons (~1 MeV) can only create low-energy recoils (up to 10 s of keV). Likewise, 10 MeV tungsten self-ions drastically over-produce very high energy recoils (up to MeV) that are not expected from fusion or fission reactors (see *fundamentally intertwined aspects* discussed above). Nevertheless, although an approximate similarity between the recoil spectrum can be seen in Figure 38, systematic evaluation of this similarity over a wide range of ion energies (Jepeal 2021) is still needed. Moreover, aspect 4 ionization effects should not be overlooked (Zhang 2020).
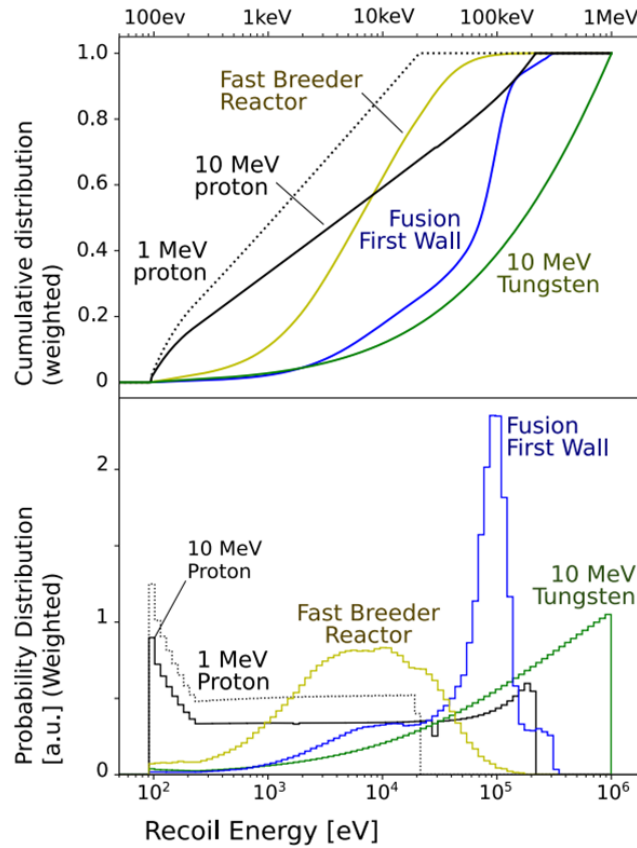

Figure 38. Comparison of several recoil spectra for tungsten: the weighted cumulative distribution function (top) and weighted probability distribution histograms (bottom) of tungsten atoms. The simulated PKA energy spectra are illustrated under example reactor neutron spectra and representative ions (Jepeal 2021).

Recoil energy spectrum for a given ion species depends strongly on its incident kinetic energy, as demonstrated by the difference between the 1 and 10 MeV proton curves in Figure 38, as well as in other examples (Figure 28, Figure 30, and Figure 32). Thus, an ion irradiation experiment can be tailored to better match the expected material response in the real-world application by carefully selecting the incident ion kinetic energy.

Four highlights are summarized by Jepeal (Jepeal 2021): (1) 5–40 MeV protons create 100 eV –1 MeV recoils with a weighted mean of ~100 keV, matching fission and fusion reactor neutrons, (2) irradiation of Fe, W, Ni, and Cu by 5–20 MeV protons creates up to ~100 app/dpa of He, equivalent to fusion reactor neutrons, (3) intermediate-energy protons can achieve 0.1-1 dpa/day in 100-300 μm samples without substantial temperature gradients, and (4) 12 MeV proton irradiation of 250 μm thick alloy 718 produces bulk tensile strengthening in agreement with reactor irradiation.